Superprotonic Conductivity in RbH<sub>2-3y</sub>(PO<sub>4</sub>)<sub>1-y</sub>: a Phosphate Deficient Analog to Cubic CsH<sub>2</sub>PO<sub>4</sub> in the (1-x)RbH<sub>2</sub>PO<sub>4</sub> – xRb<sub>2</sub>HPO<sub>4</sub> System

Grace Xiong, Louis S. Wang, and Sossina M. Haile

Department of Materials Science and Engineering, Northwestern University, Evanston, IL 60208

# **Abstract**

In contrast to CsH<sub>2</sub>PO<sub>4</sub> (cesium dihydrogen phosphate, CDP), a material with a well-established superprotonic transition to a high conductivity state at 228°C, RbH<sub>2</sub>PO<sub>4</sub> (rubidium dihydrogen phosphate, RDP) decomposes upon heating under ambient pressure conditions. Here we find, from study of the  $(1-x)RbH_2PO_4 - xRb_2HPO_4$  system, the remarkable occurrence of cubic, offstoichiometric RbH<sub>2-3 $\nu$ </sub>(PO<sub>4</sub>)<sub>1- $\nu$ </sub>, or  $\alpha$ -RDP, with a variable Rb:PO<sub>4</sub> ratio. Materials were characterized by simultaneous thermal analysis and in situ X-ray powder diffraction performed under high steam partial pressure, from which the phase diagram between RbH<sub>2</sub>PO<sub>4</sub> (x = 0) and Rb<sub>5</sub>H<sub>7</sub>(PO<sub>4</sub>)<sub>4</sub> ( $x = \frac{1}{4}$ ) was established. The system displays eutectoid behavior, with a eutectoid transition temperature of 242.0 $\pm$ 0.5 °C and eutectoid composition of  $x = 0.190 \pm 0.004$ . Even the end-member Rb<sub>5</sub>H<sub>7</sub>(PO<sub>4</sub>)<sub>4</sub> appears to transform to  $\alpha$ -RDP, implying y in the chemical formula of 0.2 and a phosphate site vacancy concentration as high as 20%. Charge balance is attained by a decrease in the average number of protons on the remaining phosphate groups. The cubic lattice parameter at x = 0.180, near the eutectoid composition, and at a temperature of 249 °C is 4.7138(2) Å. This value is substantially smaller than the estimated ambient-pressure lattice parameter of stoichiometric RbH<sub>2</sub>PO<sub>4</sub> of 4.837(12) Å, consistent with the proposal of phosphate site vacancies in the former. The superprotonic conductivity of the x = 0.180 material is  $6 \times 10^{-3}$ S/cm at 244°C, a factor of three lower than that of CDP at the same temperature. While the engineering properties of  $\alpha$ -RDP do not suggest immediate technological relevance, the discovery of a superprotonic solid acid with a high concentration of phosphate site vacancies opens new avenues for developing proton conducting electrolytes, and in particular, for controlling their transition behavior.

# Introduction

Superprotonic solid acids are materials in which high proton conductivity results from high levels of structural disorder within an otherwise crystalline framework. In such materials, proton-bearing polyanion groups undergo rapid reorientations, which, along with proton transfer between the anion groups, facilitate long-range proton motion. Typically, the disordered superprotonic phase emerges upon heating to moderate temperatures (100 – 250° C). Amongst materials in this class, CsH<sub>2</sub>PO<sub>4</sub> has received the greatest attention for potential technological applications because of its chemical stability under both oxidizing and reducing conditions. Sulfate and selenate superprotonic compounds, of which many are known (including CsHSO<sub>4</sub>) and Rb<sub>3</sub>H(SeO<sub>4</sub>)<sub>2</sub><sup>11</sup>, and even mixed sulfate-phosphate compounds such as Cs<sub>3</sub>(HSO<sub>4</sub>)<sub>2</sub>(H<sub>2</sub>PO<sub>4</sub>)<sup>12</sup>), are readily reduced upon exposure to H<sub>2</sub>, rendering them unsuitable for fuel cell and other electrochemical applications. Accordingly, efforts to expand the chemical space of technologically relevant superprotonic electrolytes remain focused on phosphate materials.

The number of known solid acid phosphate candidates is small. The closest analog to  $CsH_2PO_4$  -  $RbH_2PO_4$  - requires pressures above 1 atm to fully stabilize the cubic, superprotonic phase against dehydration, <sup>14, 15</sup> while substitutions of Cs by Rb and K in  $CsH_2PO_4$  have not yielded technologically valuable materials. <sup>16</sup> The phosphate analogs to  $Rb_3H(SeO_4)_2$  -  $Rb_3H_3(PO_4)_2$  and  $Cs_3H_3(PO_4)_2$  - do not undergo superprotonic transitions prior to decomposition, even under high steam pressure (though the superprotonic phase may yet be stabilized under high total pressure as is the case in  $RbH_2PO_4$  <sup>14, 15</sup>). Furthermore, the compound  $Ba_2KH(PO_4)_2$ , despite being essentially isostructural to superprotonic  $Rb_3H(SeO_4)_2$ , does not have particularly high conductivity. <sup>19</sup> While these lines of investigation have not proven fruitful, a recent, promising approach to the development of new phosphate based superprotonic electrolytes based on 'off-stoichiometric' compositions<sup>20</sup> or 'heterogeneous doping' has emerged. Here, one pursues materials in which the cation:polyanion atomic ratio deviates from the canonical values of 1:1 as found in the  $xCsHSO_4 - (1-x)CsH_2PO_4$  series of compounds<sup>12, 22-24</sup> and of 3:2 as found in  $A_3H(XO_4)_2$  (A = Cs, Rb,  $NH_4$ , K; X = S, Se)<sup>11</sup> and  $A_3H_3(PO_4)_2$ 0 compounds.

Following this approach, we recently reported the phase behavior of the CsH<sub>2</sub>PO<sub>4</sub> – CsH<sub>5</sub>(PO<sub>4</sub>)<sub>2</sub> system.<sup>20</sup> Amongst the phases formed in this rich chemical system is the superprotonic

compound Cs<sub>7</sub>(H<sub>4</sub>PO<sub>4</sub>)(H<sub>2</sub>PO<sub>4</sub>)<sub>8</sub>, which occurs at a Cs:PO<sub>4</sub> ratio of 7:9 and temperatures between 90 and 190 °C.<sup>25</sup> Rather remarkably, the CsH<sub>2</sub>PO<sub>4</sub> and Cs<sub>7</sub>(H<sub>4</sub>PO<sub>4</sub>)(H<sub>2</sub>PO<sub>4</sub>)<sub>8</sub> compounds exhibit eutectoid behavior, forming a non-stoichiometric cubic superprotonic phase of composition stoichiometry Cs<sub>1-x</sub>H<sub>2+x</sub>PO<sub>4</sub> over a wide range in *x*.<sup>20</sup> In parallel, Gaydamaka et al. have pursued an analogous study of the RbH<sub>2</sub>PO<sub>4</sub> – Rb<sub>2</sub>HPO<sub>4</sub> system.<sup>26</sup> These authors have reported that the compound Rb<sub>5</sub>H<sub>7</sub>(PO<sub>4</sub>)<sub>4</sub>, with a cation:polyanion ratio of 5:4, undergoes a superprotonic transition at ~237° C at which the conductivity rises from ~10<sup>-5</sup> to ~10<sup>-2</sup> S/cm, and the activation energy for proton transport becomes ~0.9 eV.<sup>27</sup> Materials with intermediate compositions between RbH<sub>2</sub>PO<sub>4</sub> and Rb<sub>5</sub>H<sub>7</sub>(PO<sub>4</sub>)<sub>4</sub> were furthermore shown to display enhanced conductivity over that of the end-members. To date, the structure of the high conductivity phase of Rb<sub>5</sub>H<sub>7</sub>(PO<sub>4</sub>)<sub>4</sub> has not been reported, nor have the materials at intermediate composition been fully characterized.

The present study was undertaken with the objective of clarifying the phase behavior in the (1-x) RbH<sub>2</sub>PO<sub>4</sub> – x Rb<sub>2</sub>HPO<sub>4</sub> system in the chemical space from RbH<sub>2</sub>PO<sub>4</sub> (x = 0) to Rb<sub>5</sub>H<sub>7</sub>(PO<sub>4</sub>)<sub>4</sub> ( $x = \frac{1}{4}$ ). Using a combination of thermal analysis, in situ x-ray powder diffraction, and impedance spectroscopy, we firmly establish bulk superprotonic conductivity in this system, distinct from the influence of heterogeneous, secondary phases. We find that, across the entire chemical space, the superprotonic phase is cubic. This cubic phase displays variable stoichiometry, best described by the formula RbH<sub>2-3y</sub>(PO<sub>4</sub>)<sub>1-y</sub> with y reaching at least 0.2 and has the surprising capacity to host vacancies on its polyanion sites.

# **Methods**

Three precursor compounds were synthesized and used for studies in the RbH<sub>2</sub>PO<sub>4</sub>-Rb<sub>5</sub>H<sub>7</sub>(PO<sub>4</sub>)<sub>4</sub> system. The first, tetragonal RbH<sub>2</sub>PO<sub>4</sub> (rubidium dihydrogen phosphate, or RDP), was prepared through methanol-induced precipitation from stoichiometric aqueous solutions of the precursors H<sub>3</sub>PO<sub>4</sub> and Rb<sub>2</sub>CO<sub>3</sub>. The second, the compound Rb<sub>2</sub>HPO<sub>4</sub>•2H<sub>2</sub>O, was prepared through evaporation-induced precipitation from stoichiometric aqueous solutions of H<sub>3</sub>PO<sub>4</sub> and Rb<sub>2</sub>CO<sub>3</sub>. The synthesis of the third, Rb<sub>5</sub>H<sub>7</sub>(PO<sub>4</sub>)<sub>4</sub>, was achieved through a high humidity precipitation route using RbH<sub>2</sub>PO<sub>4</sub> and Rb<sub>2</sub>HPO<sub>4</sub>•2H<sub>2</sub>O as the reagents. Stoichiometric quantities of these two phosphates were placed in a quartz boat and the mixture was heated in a furnace to 105°C. A steam partial pressure (*p*H<sub>2</sub>O) of 0.83 atm was introduced at this temperature, at which condition

the reagents deliquesced. Precipitation of  $Rb_5H_7(PO_4)_4$  was then induced by heating the solution to  $130^{\circ}C$  under dry  $N_2$ . The  $RbH_2PO_4$  and  $Rb_5H_7(PO_4)_4$  compounds, used in the subsequent study of phase behavior, were stored at  $85^{\circ}C$  to prevent absorption of water from the environment. Characterization was performed on materials of global composition  $Rb_{1+x}H_{2-x}PO_4$ , prepared by mixing stoichiometric quantities of the  $RbH_2PO_4$  (x=0) and  $Rb_5H_7(PO_4)_4$  ( $x=\frac{1}{4}$ ) precursors. As  $RbH_2PO_4$  has been reported upon extensively in the literature, it was not evaluated in any depth here.

Simultaneous thermal analysis (STA) was carried out using a differential scanning calorimeter/thermogravimetric analyzer (DSC/TGA) Netzsch STA 449F3. Twelve compositions ( $x = 0.020, 0.026, 0.034, 0.0625, 0.083, 0.110, 0.125, 0.143, 0.167, 0.182, 0.220, and <math>\frac{1}{4}$ , with an uncertainty in x of  $\sim 0.003$ ) were examined. For each measurement, a finely ground sample, 40 mg in mass, was lightly compacted into a Pt sample pan. Samples were heated at 1 °C/min to 350 °C, initially under dry Ar (93 sccm). At 130 °C, samples were held at this temperature for two hours and then 8.1 g/h of water vapor, used to achieve  $pH_2O = 0.7$  atm, was introduced to the system.

High temperature (in situ) powder X-ray diffraction (HTXRD) patterns were collected from 135 to 249 °C using a Smartlab 9 kW Gen 3 instrument equipped with an Anton Paar XRK 900 furnace. After combining precursors and grinding, the prepared samples were placed into the sample holder of the XRK 900 furnace and spun during measurement. Humidified gas was introduced at 135°C using a heated, humidified  $N_2$  gas line to achieve  $pH_2O = 0.83$  atm. Data were collected at 35°C intervals from 25 °C to 135 °C with a 10°C/min heating rate between measurements. From 135°C to 235°C, the sample was heated at a rate of 5 °C/min and data were collected at 25°C intervals. At higher temperatures, from 235 °C to 249 °C, the sample was heated at a rate of 2 °C/min and data were collected at 2 °C intervals. Measurements were made of five compositions (x = 0.125, 0.150, 0.180, 0.200, 0.250), supplemented with some limited studies of RbH<sub>2</sub>PO<sub>4</sub> (x = 0). For the  $x = \frac{1}{4}$  end-member, the humidity was increased to  $pH_2O = 0.88$  atm upon reaching 180 °C. Comparisons to the thermal results indicated the true temperatures within the XRK 900 furnace were approximately 5 °C higher than the set values, with a spatial variation across the sample of similar magnitude. The estimated true (average) temperatures are reported hereafter. Diffraction patterns were analyzed using the Rietveld

method in the GSAS-II program with the background, sample displacement, lattice parameters, and phase fractions refined.<sup>28</sup> Instrument profile parameters were fixed to values measured independently using the standard, lanthanum hexaboride. Structural models for the known stoichiometric compounds RbH<sub>2</sub>PO<sub>4</sub>(monoclinic)<sup>29</sup> and Rb<sub>5</sub>H<sub>7</sub>(PO<sub>4</sub>)<sub>4</sub><sup>30</sup> were employed without refinement of atomic parameters. The refinement strategy employed for the newly discovered cubic phase is described below alongside the structure descriptions.

Conductivity was measured for the composition x = 0.180 by impedance spectroscopy. The sample was formed into a pellet with a diameter of 14.85±0.03 mm and density of approximately 97% of theoretical, under a two-step uniaxial pressing protocol in which the material was pressed at 49 kPa for five min then 98 kPa for an additional five min. The surfaces of the resulting pellet were sanded using 1200 and 2000 grit sandpaper to ensure smoothness; the final pellet thickness was 0.92±0.03 mm. Platinum electrodes, 15 nm in thickness, were sputtered onto either side using a Denton Desktop Sputter IV. Impedance data were collected over the temperature range 70 to 244 °C using an 4284A Agilent LCR analyzer over a frequency range of 0.1 to 10<sup>6</sup> Hz and a voltage amplitude of 20 mV. Between 70 and 130 °C, the sample environment was exposed to a dry N<sub>2</sub> gas stream (40 sccm); between 130 and 180 °C, the gas stream was humidified to 0.83 atm pH<sub>2</sub>O; and above 180 °C, the atmosphere was increased to 0.88 pH<sub>2</sub>O (balance N<sub>2</sub>). The total flow rate was kept constant throughout the experiment. Data were collected in 10 °C intervals between 70 and 180 °C using a heating rate of 5 °C/min between measurements. Data between 180 and 244 °C were collected at 5-10 °C intervals with a heating rate of 2 °C/min between steps. At each measurement condition, samples were allowed to equilibrate for 30 mins before recording the impedance spectrum. The impedance data were analyzed using the commercial software package ZView.

As is the norm for crystallographic studies, all estimated uncertainties are reported in parentheses and reflect the uncertainty in the final digit(s) of the quoted values.

# **Results and Discussion**

#### **Phase Behavior**

The (1-x)RbH<sub>2</sub>PO<sub>4</sub> – xRb<sub>2</sub>HPO<sub>4</sub> phase diagram ( $0 \le x \le 0.25$ ) shown in Figure 1 was determined on the basis of the thermal analysis and diffraction measurements. Though Rb<sub>5</sub>H<sub>7</sub>(PO<sub>4</sub>)<sub>4</sub> was used in material preparation, for notational ease, Rb<sub>2</sub>HPO<sub>4</sub> (the anhydrous product of heating Rb<sub>2</sub>HPO<sub>4</sub>•2H<sub>2</sub>O to the temperatures of reported in Figure 1) is specified as the end member compound of the phase diagram theanhydrous. At temperatures between 125 and 241 °C, the stoichiometric compound Rb<sub>5</sub>H<sub>7</sub>(PO<sub>4</sub>)<sub>4</sub> was found to coexist with stoichiometric, monoclinic RbH<sub>2</sub>PO<sub>4</sub> (space group  $P2_1/m$ ), as demonstrated in the representative diffraction patterns for several compositions collected at (or close to) 235 °C, Figure S1. Tetragonal RbH<sub>2</sub>PO<sub>4</sub> transforms to the monoclinic phase at ~109 °C<sup>31</sup> and is thus not represented in the phase diagram of Figure 1. Gaydamaka reported a similar co-existence of Rb<sub>5</sub>H<sub>7</sub>(PO<sub>4</sub>)<sub>4</sub> and RbH<sub>2</sub>PO<sub>4</sub> phases, without reactions between the two, for x = 0.1 and 0.2 global compositions, albeit with RbH<sub>2</sub>PO<sub>4</sub> in the tetragonal form due to the ambient temperature measurement. <sup>26</sup> The mutual insolubility of Rb<sub>5</sub>H<sub>7</sub>(PO<sub>4</sub>)<sub>4</sub> and RbH<sub>2</sub>PO<sub>4</sub> is evident from the insensitivity of the high temperature unit cell volumes of these materials to the presence of the other phase (Figure S2, Table S1-S3).

#### Eutectoid Reaction and Formation of α-RbH<sub>2</sub>PO<sub>4</sub>

Upon heating, Rb<sub>5</sub>H<sub>7</sub>(PO<sub>4</sub>)<sub>4</sub> and RbH<sub>2</sub>PO<sub>4</sub>(m) were found to undergo a reaction at 242 °C, reflected, for example, in the DSC/TGA profiles of the representative compositions x = 0.026 and 0.182 (pH<sub>2</sub>O = 0.7 atm), Figure 2. Though the reaction is followed closely by mass loss, the reaction itself precedes any mass change. Shown on the phase diagram of Figure 1 are the reaction temperatures determined from the 12 discrete x values, with the corresponding DSC/TGA profiles reported in Figure S3. In each case, a thermal anomaly is detected that precedes mass loss. Excluding the end-member composition  $x = \frac{1}{4}$ , the anomaly occurs at 242.0(5) °C. We attribute the thermal event to a eutectoid, solid state reaction between Rb<sub>5</sub>H<sub>7</sub>(PO<sub>4</sub>)<sub>4</sub> and RbH<sub>2</sub>PO<sub>4</sub>(m) to form a solid product phase.

The nature of the phase that appeared at 242 °C was established from the *in situ* diffraction studies. Shown in Figure 3 and Figure 4 are representative sets of diffraction patterns for the x = 0.200 and x = 0.180 compositions, respectively. The complete sets of patterns for these

compositions (all measurement temperatures) are shown in Figure S4, with refined cell parameters and phase fractions reported in Tables S4 and S5. As indicated in Figure 1, these representative compositions lie on either side of the eutectoid composition, identified below as occurring at  $x \approx 0.190$ .

The diffraction measurement of the hypereutectic composition (x = 0.200), Figure 3, shows that the two-phase mixture of stoichiometric Rb<sub>5</sub>H<sub>7</sub>(PO<sub>4</sub>)<sub>4</sub> and RbH<sub>2</sub>PO<sub>4</sub>(m) indicate in the phase diagram, Figure 1, is retained to a temperature of 241 °C. At 247 °C (the next temperature at which data were recorded for this composition), the pattern changes markedly, indicative of the phase transformation detected by thermal analysis. At 249 °C all peaks can be indexed to a primitive cubic cell with lattice constant 4.702(1) Å, with no remaining peaks from either precursor.

In the case of the hypoeutectoid composition (x = 0.180), Figure 4, analogous behavior is observed. The phases Rb<sub>5</sub>H<sub>7</sub>(PO<sub>4</sub>)<sub>4</sub> and RbH<sub>2</sub>PO<sub>4</sub>(m) are retained to 235 °C (the highest measurement temperature below the eutectoid transition). At 245 °C, the pattern is dominated by a primitive cubic phase, and at 249 °C, all peaks can be indexed to this cell. The cubic lattice at this composition is 4.7138(2) Å (at 249 °C). Rather remarkably, the new cubic phase, as revealed by Rietveld refinement, is isostructural to superprotonic CsH<sub>2</sub>PO<sub>4</sub> (sp. grp.  $Pm\bar{3}m$ ). This nonstoichiometric phase, with global composition Rb<sub>1+x</sub>H<sub>2-x</sub>PO<sub>4</sub>, is hereafter referred to as  $\alpha$ -RDP. The phase diagram, Figure 1, provides a summary of the diffraction results. No phases other than those indicated were observed under any condition examined.

Beyond revealing the occurrence of a solid state reaction at 242 °C, the thermal measurements showed consistency with a eutectoid composition of  $x \ge 0.14$ . The measured enthalpy of the eutectoid transition (deconvoluted from the dehydration enthalpy by peak fitting, Figure S5) generally increased as x increased over the range from 0.020 to 0.143, Figure 5, rising from 1.5 kJ/mol to 11.7 kJ/mol, where the enthalpy values have been normalized to the moles of Rb<sub>1+x</sub>H<sub>2-x</sub>PO<sub>4</sub>. The increase occurs because the fraction of material undergoing the transformation monotonically increases as x approaches x<sub>eutectoid</sub>. In the range 0.14 < x < 0.22 the overlap between the eutectoid transition and dehydration events was too severe to permit accurate measurement of the eutectoid transition enthalpy (see Figure 2b for example). Accordingly, data

collected at higher x values are omitted from Figure 5. Extrapolation to x = 0.180-0.200 suggests an enthalpy of reaction of  $\approx 15$ -16 kJ/mol(Rb<sub>1+x</sub>H<sub>2-x</sub>PO<sub>4</sub>).

Heating of the (1-x)RbH<sub>2</sub>PO<sub>4</sub> – xRb<sub>2</sub>HPO<sub>4</sub> materials in the thermal analysis experiments to even just a few degrees beyond the eutectoid temperature resulted in mass loss, which was accompanied by a thermal signature, as in the example of the x = 0.182 composition, Figure 2b. The initiation of dehydration shifted slightly to lower temperatures with increasing x, from 249.2 °C at x = 0.020 to 244.9 °C at  $x = \frac{1}{4}$  under pH<sub>2</sub>O = 0.7 atm (Figure S2). Thus,  $\alpha$ -RDP exists only over a narrow temperature window, even at very high H<sub>2</sub>O partial pressure. It is known that stoichiometric RbH<sub>2</sub>PO<sub>4</sub> cannot be stabilized in the superprotonic cubic structure at any H<sub>2</sub>O pressure below 1 atm.<sup>31</sup> Hence, it is not surprising that  $\alpha$ -RDP would undergo ready dehydration.

At temperatures between the eutectoid and the solvus temperatures, the diffraction patterns of the hypoeutectoid compositions generally revealed the presence of the two expected phases – RbH<sub>2</sub>PO<sub>4</sub>(m) and  $\alpha$ -RDP. Analysis of the phase fractions in these regions enabled further narrowing of the range for the eutectoid composition. Specifically, at x = 0.180 and T = 245 °C (Figure 4b), Rietveld refinement revealed the mass percentage of  $\alpha$ -RDP to be 96.3(5) %. Application of the phase rule and an assumption of stoichiometric Rb<sub>5</sub>H<sub>7</sub>(PO<sub>4</sub>)<sub>4</sub>, imply the  $\alpha$ -RDP phase to have a composition of x = 0.1868(9), and thus  $x_{\text{eutectoid}}$  must exceed this value. Due to temperature variations across the sample stage, the phase behavior in the hypereutectic region could not be fully discerned on the basis of the diffraction data alone. Despite some uncertainty in the temperature, the behavior of the x = 0.200 composition sets an upper bound for the eutectoid composition. Specifically, at a nominal temperature of 247 °C (Figure 3b), Rietveld refinement revealed the mass percentage of  $\alpha$ -RDP in the mixture with Rb<sub>5</sub>H<sub>7</sub>(PO<sub>4</sub>)<sub>4</sub> to be 64.77(4) %. In turn, this implies the  $\alpha$ -RbH<sub>2</sub>PO<sub>4</sub> phase occurring here to have a composition of x = 0.194(1). Thus, the eutectoid composition,  $x_{\text{euc}}$ , is limited to  $0.187 < x_{\text{euc}} < 0.194$  and is taken hereafter to be at the center of this range, with value 0.190(4).

#### **Properties of the End-Member Compounds and the Solvus Lines**

The thermal behavior of the end-member material, Rb<sub>5</sub>H<sub>7</sub>(PO<sub>4</sub>)<sub>4</sub> ( $x = \frac{1}{4}$ ), showed slight but important differences from those of the intermediate compositions, Figure 6a. A large thermal

event was observed for this material at 243.2 °C, slightly higher than the mean eutectoid temperature of 242  $\pm 0.5$  °C. Furthermore, the enthalpy for this event was found to be 13.4 kJ/mol( $\alpha$ -RDP), larger than the maximum value of 11.7 kJ/mol recorded at x = 0.143 (Figure 5). These factors suggest a stoichiometric transition of Rb<sub>5</sub>H<sub>7</sub>(PO<sub>4</sub>)<sub>4</sub> into α-RDP, similar to what has been observed for the transition of  $Cs_7(H_4PO_4)(H_2PO_4)_8$  into  $\alpha$ -CDP. <sup>20, 25</sup> The diffraction data (reported in full in Figure S6 and Table S6) revealed a simple cubic pattern at 249 °C with cell parameter 4.7028(5) Å, Figure 6c, consistent with the occurrence of  $\alpha$ -RDP and with the proposed phase diagram. However, the Rb<sub>5</sub>H<sub>7</sub>(PO<sub>4</sub>)<sub>4</sub> phase appeared to be retained up to 247 °C, Figure 6b. While the possibility that this reflects a true feature of the material system (which is treated here as binary system despite the chemical complexity) cannot be entirely ruled out, we assign the observation of Rb<sub>5</sub>H<sub>7</sub>(PO<sub>4</sub>)<sub>4</sub> at temperatures beyond the stoichiometric transition temperature of 243 °C to cold spots in the heating stage. Additionally, slow kinetics due to poor heat transfer between loosely contacted particles (in contrast to the light compaction employed for the thermal analysis) may have contributed to a sluggish transformation. On the basis of conductivity measurements (but no crystallographic studies), Gaydamaka reported a superprotonic transition at 237 °C in Rb<sub>5</sub>H<sub>7</sub>(PO<sub>4</sub>)<sub>4</sub><sup>27</sup>, consistent with the structural transition proposed here.

With the stoichiometric transition temperature for  $Rb_5H_7(PO_4)_4$  so estimated, the solvus line in the hypereutectoid region is taken to be linear between this transition and the eutectoid position. Similarly, in the hypoeuctectoid region, the solvus line is taken to be linear between the eutectoid point and the superprotonic transition of stoichiometric  $RbH_2PO_4$ . The latter is  $\approx 280$  °C, as measured by thermal analysis by both Gaydamaka<sup>26</sup> (onset at 255 °C, peak at 283 °C) and  $Li^{31}$  (peak at 276 °C). In both studies, despite kinetic competition from dehydration, the polymorphic transition to cubic RDP was reliably detected. Attempts to evaluate the solvus line by application of the phase rule to diffraction patterns collected in the two-phase region were unsuccessful due to the sensitivity of the results to the slight variations in the stage temperature and, at temperatures well above the eutectoid transition, due to the ready dehydration of the material.

#### Structure of \alpha-RDP

The global composition of  $\alpha$ -RDP, with a Rb/PO<sub>4</sub> ratio > 1, appears at first glance, to be incompatible with the superprotonic CsH<sub>2</sub>PO<sub>4</sub> structure type (sp. grp.  $Pm\bar{3}m$ ), in which Cs atoms adopt a simple-cubic arrangement and the polyanion units occupy the cube center positions.<sup>32, 33</sup> This structure, a derivative of the CsCl structure, does not have interstitial sites of sufficient size and appropriate coordination environment to host large alkali atom species and thus accommodate the Rb excess in  $\alpha$ -RDP. For example, possible sites at  $(\frac{1}{2}, \frac{1}{2}, 0)$ , and  $(\frac{1}{4}, \frac{1}{4}, \frac{1}{$ 1/4) have cations in the nearest neighbor coordination sphere. Furthermore, if Rb excess were to be accommodated by Rb interstitials, one would expect the cell parameter to increase with x. The observation here, however, is a decrease in cell parameter in  $\alpha$ -RDP from an estimated value of 4.837(12) Å for the hypothetical stoichiometric material (Figure S7) to an average of 4.706  $\pm$ 0.006 Å across the three compositions of finite x (and T = 249 °C). As an alternative to Rb interstitial incorporation, one can consider the formation of Rb  $\leftrightarrow$  PO<sub>4</sub> antisite defects, in which Rb cations replace H<sub>2</sub>PO<sub>4</sub> anions as a means of accommodating the Rb excess in α-RDP. While not inconsistent with the cell contraction, cation/anion antisite defects carry an extremely large electrostatic energy penalty in an ionic material, even with next nearest phosphate groups serving as the sites from which protons are lost to achieve overall charge balance. Accordingly, antisite defects are unlikely to be the means by which the nonstoichiometry is realized. With these possibilities eliminated, we suggest that the material achieves Rb excess by hosting vacancies on the anion sites. Here, the overall charge balance is maintained by removal of additional protons from other H<sub>2</sub>PO<sub>4</sub> groups. In this scenario, the chemical formula of the cubic phase is described as  $RbH_{2-3\nu}(PO_4)_{1-\nu}$  rather than by the global composition of  $Rb_{1+x}H_{2-x}PO_4$ . The cell contraction then reflects the loss of large anion groups and local contraction about the anion vacancies.

Shown in Figure 7 is the structure of  $\alpha$ -RDP at x = 0.18 and 245 °C, corresponding to the refinement presented in Figure 4b. Associated crystallographic results are summarized in Table 1. The structure of cubic CsH<sub>2</sub>PO<sub>4</sub> was used as a starting model in the analysis and the following steps were taken in the refinement. The lattice parameter and isotropic displacement parameters for the Rb and P atoms were allowed to vary freely. The isotropic displacement parameter for O was then set to a value 7% larger than that of P, in analogy to the properties of cubic CsH<sub>2</sub>PO<sub>4</sub>, <sup>33</sup> and the oxygen position refined with a restraint targeting a P-O bond length of 1.53 Å.

Additionally, as alluded to above, a small amount of RbH<sub>2</sub>PO<sub>4</sub>(m) was detected in this pattern (< 4 wt. %), and the relative amounts of the two phases was freely refined. As with the lower temperature refinements, the instrument profile parameters were fixed at the reference values obtained from a measurement of LaB<sub>6</sub>, whereas the sample displacement was freely varied. In all cases in which the  $\alpha$ -RDP phase was detected, the diffraction peaks from this material were slightly broadened relative to those of the other phases. This feature was treated by refining the  $\alpha$ -RDP crystalline size. Peak broadening is plausibly explained by the presence of anion vacancies which would give rise to a distribution in interatomic distances. The final refinement statistics for the refinement indicated in Figure 4b,  $R_{\rm wp} = 6.24\%$  and GooF = 7.56, along with the overall features of the difference pattern, indicate the satisfactory nature of the model. The final  $R_{\rm F}$  ( $R_{\rm Bragg}$ ) for the  $\alpha$ -RDP phase was 7.89%. The model captures the diffraction features of the x = 0.200 composition at 249° C (Figure 3c) particularly well.

Similar to stoichiometric cubic CsH<sub>2</sub>PO<sub>4</sub>, the polyanion groups at the unit cell center of  $\alpha$ -RDP can adopt one of several different orientations, and an example of one possible orientation is shown in Figure 7b. In the stoichiometric material, the mean oxygen site occupancy is 1/6, and this has been interpreted to correspond to six possible orientations.<sup>3</sup> For the material  $\alpha$ -RDP with x = 0.18, 15 % of the anion sites are vacant according to the proposed structural interpretation, implying an oxygen site occupancy of 0.14. Given the limited number of diffraction peaks and the possibility of poor powder randomization due to crystallite coarsening on heating, refinement of the P and O site occupancies to confirm the hypothesis of anion site vacancies was not possible. Instead, the occupancies were fixed in the Rietveld analysis at the values expected for the proposed structural model and ignoring the small impact on  $\alpha$ -RDP stoichiometry of the presence of residual RbH<sub>2</sub>PO<sub>4</sub>(m) in this pattern. Refinements at higher temperatures, at which RbH<sub>2</sub>PO<sub>4</sub>(m) was completely consumed but the diffraction data were slightly obscured by a higher background signal, produced similar results, Table S5. In the case of the end member compound Rb<sub>5</sub>H<sub>7</sub>(PO<sub>4</sub>)<sub>4</sub>, stoichiometric transformation to  $\alpha$ -RDP implies, rather remarkably, that the structure is stable with as much as 20% of the polyanion sites unoccupied.

#### **Superprotonic Conductivity**

The conductivity of the Rb<sub>1+x</sub>H<sub>2-x</sub>PO<sub>4</sub> material with x = 0.18 (near the eutectoid composition) increased sharply between 230 and 238 °C, rising by over two orders of magnitude across this

narrow temperature window, Figure 8. The behavior is directly evident in the raw impedance spectra (Figure S8). While there is a slight offset from the transition temperature of 241 °C measured by thermal analysis, the increase in conductivity is consistent with the proposed eutectoid transition to superprotonic  $\alpha$ -RDP. At the highest temperature of measurement, 244°C, the conductivity is  $6 \times 10^{-3}$  S/cm, similar to that estimated for stoichiometric RbH<sub>2</sub>PO<sub>4</sub> ( $7 \times 10^{-3}$ S/cm), Figure S9, and somewhat lower than that of CsH<sub>2</sub>PO<sub>4</sub> ( $2 \times 10^{-2}$  S/cm) at a comparable temperature. 16 As is typical of superprotonic transformations, 21 the reverse transition to the low conductivity state was sluggish on cooling. Here, the reverse reaction involves disproportionation into the two precursor phases, a process that presumably adds to the commonly observed hysteresis. The conductivity of the metastable state displayed linear behavior in an Arrhenius plot between 230 and 244°C, from which the activation energy, E<sub>a</sub>, and preexponential factor ln(A) for proton transport in the expression  $\sigma = \frac{A}{T} exp\left(\frac{E_a}{k_B T}\right)$  (where T is temperature and  $k_b$  is Boltzmann's constant) were obtained. The resulting values are 0.57 eV and 13.84 S/cm K, respectively, both larger than the corresponding terms in CsH<sub>2</sub>PO<sub>4</sub> (0.384 eV and 11.32 S/cm K). <sup>16</sup> Thus, over the narrow temperature range of stability of α-RDP, the higher activation energy overwhelms the benefits of a higher preexponential factor and results in a lower conductivity than that of CsH<sub>2</sub>PO<sub>4</sub>.

#### **Discussion**

Observation of a phase isostructural to superprotonic CsH<sub>2</sub>PO<sub>4</sub> with a large concentration of phosphate group vacancies is surprising, but fully supported by the experimental results. In particular, the diffraction data reveal the transformation of all compositions near the eutectoid to a cubic phase at temperatures just beyond the thermal anomaly at 242 -243°C. The cell contraction relative to stoichiometric cubic RbH<sub>2</sub>PO<sub>4</sub> eliminates all other possible structural configurations. The superprotonic transitions reported by Gaydamaka et al. across the RbH<sub>2</sub>PO<sub>4</sub> – Rb<sub>2</sub>HPO<sub>4</sub> system<sup>26</sup> can be understood to reflect the formation of α-RDP.

It is of some value to evaluate the thermal and entropic signatures of the transition to  $\alpha$ -RDP. The eutectoid reaction (at x = 0.190(4) and T = 242.0(5) °C) can be written as

$$0.203 \text{ RbH}_2\text{PO}_4 + 0.159 \text{ Rb}_5\text{H}_7(\text{PO}_4)_4 \rightarrow \alpha - \text{RbH}_{1.52}(\text{PO}_4)_{0.84}$$
 (1)

from which it evident that 80 mole % of the Rb species in the product derive from Rb<sub>5</sub>H<sub>7</sub>(PO<sub>4</sub>)<sub>4</sub>, implying the reaction thermodynamics are dominated by this reactant. From the estimated enthalpy of this reaction of 15.5 kJ/mol( $\alpha$ -RDP) noted above, the entropy of reaction is 30.1 J/mol-K.

In the case of the end member compound, the stoichiometric reaction (at T = 243.2 °C) is

$$0.2 \text{ Rb}_5 \text{H}_7(\text{PO}_4)_4 \rightarrow \alpha \text{-RbH}_{1.4}(\text{PO}_4)_{0.8}$$
 (2)

The enthalpy recorded for this transition, 13.4 kJ/mol, is taken to be a lower bound for the true value due to the overlap with dehydration (as noted for compositions in the range 0.14 < x < 0.22). The corresponding transition entropy is 26.0 J/mol-K, and again reflects a minimum value. Both the enthalpy and entropy changes associated with the reactions to form  $\alpha$ -RDP are greater than those of stoichiometric CsH<sub>2</sub>PO<sub>4</sub>, 11.3 kJ/mole and 22.5 J/mol-K, respectively. Because the structures of the low temperature phases differ, monoclinic CsH<sub>2</sub>PO<sub>4</sub> vs. orthorhombic Rb<sub>3</sub>H<sub>7</sub>(PO<sub>4</sub>)<sub>4</sub> and indeed the hydrogen positions in the latter are not known<sup>30</sup>, it is not possible to readily identify the sources of the differences. However, due to the presence of anion vacancies,  $\alpha$ -RDP would be expected to have greater configurational entropy than stoichiometric, cubic CDP, and hence a larger entropy of transition to  $\alpha$ -RDP is reasonable.

The presence of phosphate group vacancies, while stabilizing the cubic structure, might be expected to negatively influence the conductivity due to the loss of proton transport pathways relative to the stoichiometric analog. On the other hand, the lower conductivity of  $\alpha$ -RDP, higher activation energy for proton transport, and larger pre-exponential factor are all consistent with what is observed in cubic CDP upon Rb doping, in which the hydrogen bond network is grossly unchanged relative to stoichiometric, cubic CDP. Thus, the specific reasons for the slightly lower conductivity of  $\alpha$ -RDP remain to be isolated.

#### **Summary and Conclusions**

The phase behavior of in the (1-x) RbH<sub>2</sub>PO<sub>4</sub> – x Rb<sub>2</sub>HPO<sub>4</sub> system in the chemical space from RbH<sub>2</sub>PO<sub>4</sub> (x = 0) to Rb<sub>5</sub>H<sub>7</sub>(PO<sub>4</sub>)<sub>4</sub> ( $x = \frac{1}{4}$ ) has been carried out by *in situ* XRD and thermal analysis under controlled atmospheres with high steam partial pressure to suppress dehydration. The system was found to display eutectoid behavior, with a eutectoid composition of x = 0.190(5) and transition temperature of 242.0(5) °C. Above the transition temperature, the

structure adopts the cubic superprotonic structure of CsH<sub>2</sub>PO<sub>4</sub>, though with a large concentration ( $\sim$ 15%) of polyanion vacancies, denoted here as  $\alpha$ -RDP. Charge balance is maintained by a concomitant reduction in the number of protons on remaining polyanion groups. The conductivity of the material of eutectic composition approaches that of superprotonic CsH<sub>2</sub>PO<sub>4</sub>. The end-member compound Rb<sub>5</sub>H<sub>7</sub>(PO<sub>4</sub>)<sub>4</sub> appears to undergo a stoichiometric transition to  $\alpha$ -RDP with a remarkable 20% polyanion vacancies. The thermal stability window of  $\alpha$ -RDP is small, rending this material unlikely to be of direct technological value. However, the surprising discovery of an off-stoichiometric superprotonic cubic phase in which cations outnumber polyanions indicates that non-stoichiometry holds promise for continued material discovery.

## **Supporting Information**

Selected diffraction patterns; cell volumes as functions of temperature; complete DSC/TGA data; estimation of cell parameter of hypothetical cubic RbH<sub>2</sub>PO<sub>4</sub> at ambient pressure; selected impedance spectra.

## Acknowledgements

Financial support has been provided by the National Science Foundation (DMR-1807234, DMR-2118201 and DGE-1842165). This work made use of the J.B. Cohen X-Ray Diffraction facility at Northwestern University, supported by the NSF MRSEC program (NSF DMR-1720139). We thank Elise Goldfine for assistance with diffraction measurements.

#### **Tables**

Table 1. Fractional atomic coordinates and displacement parameters of  $\alpha$ -Rb<sub>1+x</sub>H<sub>2-x</sub>PO<sub>4</sub> at x = 0.180 and T = 245 °C. Structure adopts space group  $Pm\overline{3}m$  with a = 4.7138(2) Å. The P-O bond distance is 1.51(2) Å. Numbers in parentheses reflect the uncertainty in the final digit(s) of the quoted values.

Atom	X	у	Z	site	occupancy	$U_{\rm iso}$ (Å <sup>2</sup> )*
Rb	0	0	0	1 <i>a</i>	1	0.068(2)
P	1/2	1/2	1/2	1 <i>b</i>	0.85	0.054(4)
O	1/2	0.203(1)	0.375(2)	24 <i>l</i>	0.14	0.058(4) <sup>b</sup>

<sup>&</sup>lt;sup>a</sup> fixed to match global chemistry

 $<sup>^{\</sup>mathrm{b}}$  tied to the  $U_{\mathrm{iso}}$  of P by a multiplicative factor of 1.073

<sup>\*</sup>Note:  $U_{iso}$  values are corrected here; published values correspond to  $\beta_{iso}$  and are incorrectly identified as  $U_{iso}$ .

## **Figure Captions**

Figure 1. Phase diagram across the (1-x) RbH<sub>2</sub>PO<sub>4</sub> – x Rb<sub>2</sub>HPO<sub>4</sub> system for  $0 \le x \le 0.25$ . Datapoints indicated with parentheses are in slight disagreement with the proposed phase boundaries, likely due to cold spots in the high-temperature XRD stage. The eutectoid transition temperature, established by thermal analysis, occurs at 242.0 ± 0.5 °C, and the eutectoid composition is  $x = 0.190 \pm 0.004$ . The eutectoid transition occurs at a significantly lower temperature than the superprotonic transition of stoichiometric RbH<sub>2</sub>PO<sub>4</sub> ( $\approx 280^{\circ}$  C<sup>26, 31</sup>).

Figure 2. DSC/TGA measurements of materials with composition (a) x = 0.026, and (b) x = 0.182, both under  $pH_2O = 0.7$  atm. In both cases, the first thermal event in the DSC signal occurs without any mass loss. Events at higher temperature align with mass loss seen in the TG signal and are accordingly attributed to dehydration.

Figure 3. Diffraction patterns and Rietveld refinements for x = 0.200 at (a) 241 °C, below the eutectoid transition, (b) 247 °C, just above the eutectoid transition, and (c) 249 °C, within the single-phase cubic region, all collected under  $pH_2O = 0.83$  atm.

Figure 4. Diffraction patterns and Rietveld refinements for x = 0.180 at (a) 235 °C, below the eutectoid transition, (b) 245 °C, just above the eutectoid transition, and (c) 249 °C, within the single-phase cubic region, all collected under  $pH_2O = 0.83$  atm.

Figure 5. Enthalpy of the eutectoid transition as a function of composition.

Figure 6. High temperature phase transition of Rb<sub>5</sub>H<sub>7</sub>(PO<sub>4</sub>)<sub>4</sub> ( $x = \frac{1}{4}$ ) revealed (a) by thermal analysis under  $pH_2O = 0.7$  atm; and by x-ray diffraction patterns collected at (b) 237°C and (c) 249°C under  $pH_2O = 0.88$  atm.

Figure 7. Proposed structure of  $\alpha$ -RDP at x near the eutectoid composition (x = 0.180) with (a) all 24 oxygen sites shown; and (b) four oxygen sites that form one of the tetrahedral group orientations shown.

Figure 8. Conductivity of  $\alpha$ -RDP at x near the eutectoid composition (x = 0.180) as measured over the temperature range of 25°C to 244°C. The jump in conductivity corresponds to the superprotonic phase transition observed in DSC and high temperature XRD measurements.

#### References

- 1. A. Baranov, *Crystallography Reports*, 2003, **48**, 1012-1037.
- 2. D. A. Boysen, T. Uda, C. R. I. Chisholm and S. M. Haile, *Science*, 2004, **303**, 68.
- 3. S. M. Haile, C. R. I. Chisholm, K. Sasaki, D. A. Boysen and T. Uda, *Faraday Discussions*, 2007, **134**, 17-39.
- 4. K. Imamura and J. Kubota, *Sustain. Energ. Fuels*, 2019, **3**, 1406-1417.
- 5. J. Otomo, S. Nishida, H. Takahashi and H. Nagamoto, *Journal of Electroanalytical Chemistry*, 2008, **615**, 84-90.
- 6. A. B. Papandrew, C. R. I. Chisholm, R. A. Elgammal, M. M. Ozer and S. K. Zecevic, *Chemistry of Materials*, 2011, **23**, 1659-1667.
- 7. O. Paschos, J. Kunze, U. Stimming and F. Maglia, *Journal of Physics-Condensed Matter*, 2011, **23**.
- 8. T. Uda, D. A. Boysen, C. R. I. Chisholm and S. M. Haile, *Electrochemical and Solid State Letters*, 2006, **9**, A261-A264.
- 9. T. Uda and S. M. Haile, *Electrochemical and Solid State Letters*, 2005, **8**, A245-A246.
- 10. A. Baranov, L. Shuvalov and N. Shchagina, *JETP Letters*, 1982, **36**, 459-462.
- 11. A. Pawlowski, C. Pawlaczyk and B. Hilczer, *Solid State Ionics*, 1990, 44, 17-19.
- 12. S. M. Haile, G. Lentz, K. D. Kreuer and J. Maier, Solid State Ionics, 1995, 77, 128-134.
- 13. R. B. Merle, C. R. I. Chisholm, D. A. Boysen and S. M. Haile, *Energy Fuels*, 2003, **17**, 210-215.
- 14. D. A. Boysen, S. M. Haile, H. J. Liu and R. A. Secco, *Chemistry of Materials*, 2004, **16**, 693-697.
- 15. C. E. Botez, R. J. Tackett, J. D. Hermosillo, J. Z. Zhang, Y. S. Zhao and L. P. Wang, *Solid State Ionics*, 2012, **213**, 58-62.
- 16. A. Ikeda, D. A. Kitchaev and S. M. Haile, *Journal of Materials Chemistry A*, 2014, **2**, 204-214.
- 17. S. Sanghvi and S. M. Haile, *Journal of Solid State Chemistry*, 2021, **296**.
- 18. S. Sanghvi and S. M. Haile, *Solid State Ionics*, 2020, **349**.
- 19. C. R. I. Chisholm, E. S. Toberer, M. W. Louie and S. M. Haile, *Chemistry of Materials*, 2010, **22**, 1186-1194.
- 20. L. S. Wang, S. V. Patel, E. Truong, Y.-Y. Hu and S. M. Haile, *Chemistry of Materials*, 2022, **34**, 1809-1820.
- 21. V. G. Ponomareva and I. N. Bagryantseva, *Solid State Ionics*, 2019, **329**, 90-94.
- 22. V. G. Ponomareva and I. N. Bagryantseva, *Inorg. Mater.*, 2012, **48**, 187-194.
- 23. Y. Yamane, K. Yamada and K. Inoue, *Solid State Ionics*, 2008, **179**, 483-488.
- 24. C. R. I. Chisholm, Ph.D., California Institute of Technology, 2003.
- 25. L. S. Wang, S. V. Patel, S. S. Sanghvi, Y. Y. Hu and S. M. Haile, *Journal of the American Chemical Society*, 2020, **142**, 19992-20001.
- 26. A. A. Gaydamaka, V. G. Ponomareva and I. N. Bagryantseva, *Solid State Ionics*, 2019, **329**, 124-130.
- 27. A. A. Gaydamaka, V. G. Ponomareva and I. N. Bagryantseva, *Ionics*, 2019, 25, 551-557.
- 28. B. H. Toby and R. B. Von Dreele, *Journal of Applied Crystallography*, 2013, **46**, 544-549.
- 29. M. T. Averbuch-Pouchot and A. Durif, *Acta Crystallographica*, 1985, C41, 665-667.
- 30. M. T. Averbuch-Pouchot and A. Durif, Acta Crystallographica 1985, C41, 1555–1556.

- 31. Z. K. Li and T. B. Tang, Mater. Res. Bull., 2010, 45, 1909-1915.
- 32. C. E. Botez, J. D. Hermosillo, J. Zhang, J. Qian, Y. Zhao, J. Majzlan, R. R. Chianelli and C. Pantea, *The Journal of Chemical Physics*, 2007, **127**, 194701.
- 33. K. Yamada, T. Sagara, Y. Yamane, H. Ohki and T. Okuda, *Solid State Ionics*, 2004, **175**, 557-562.

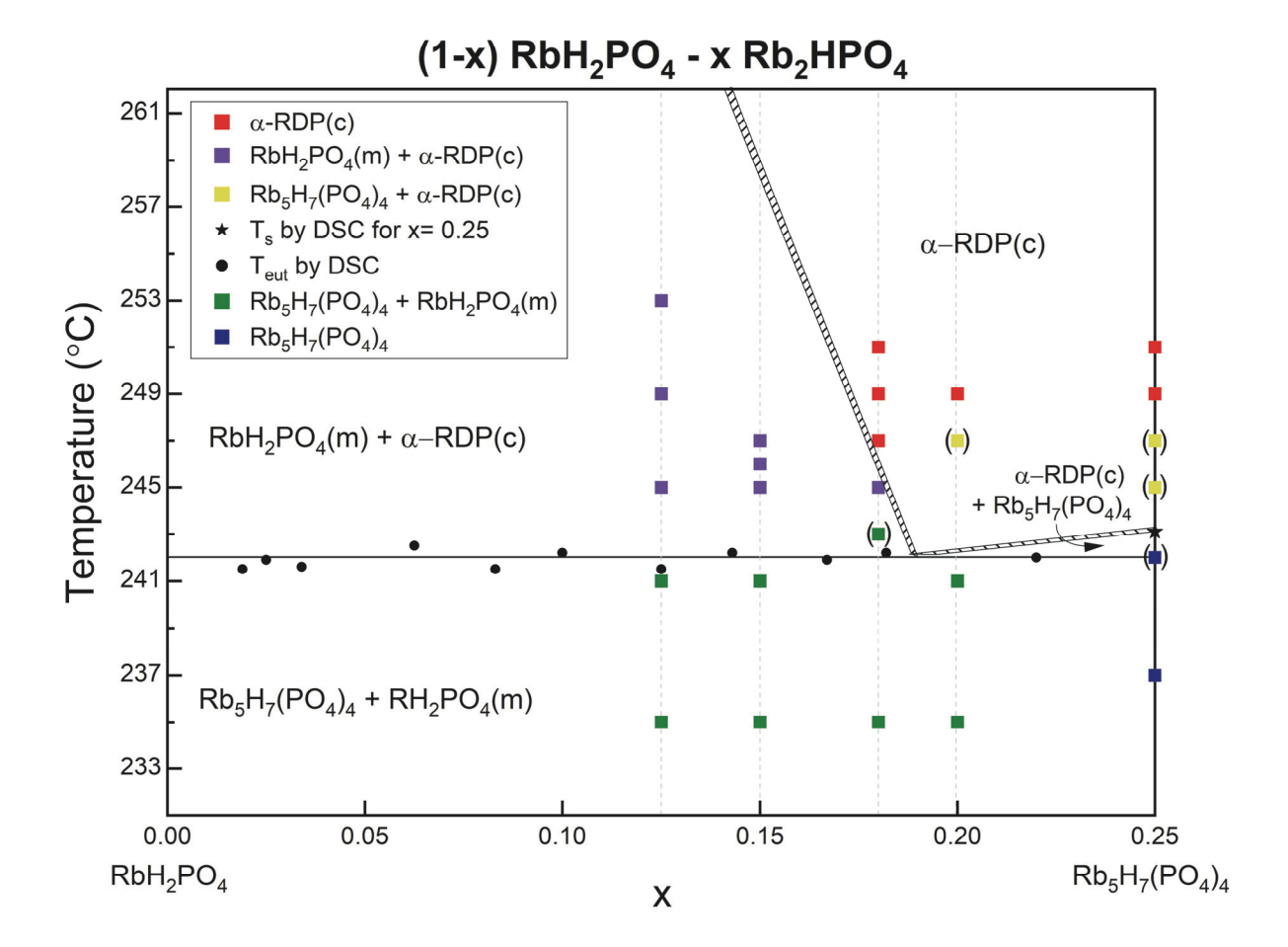


Figure 1.

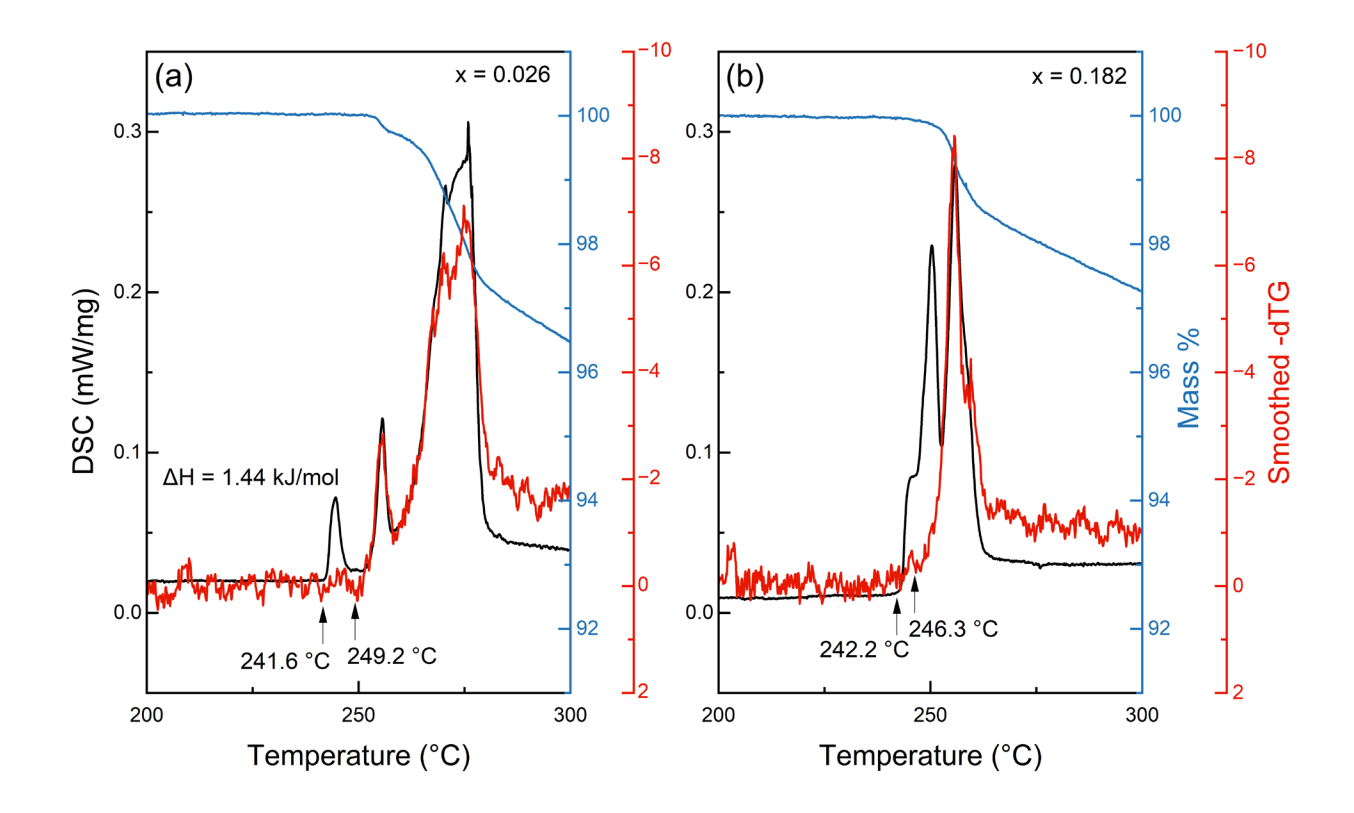


Figure 2.

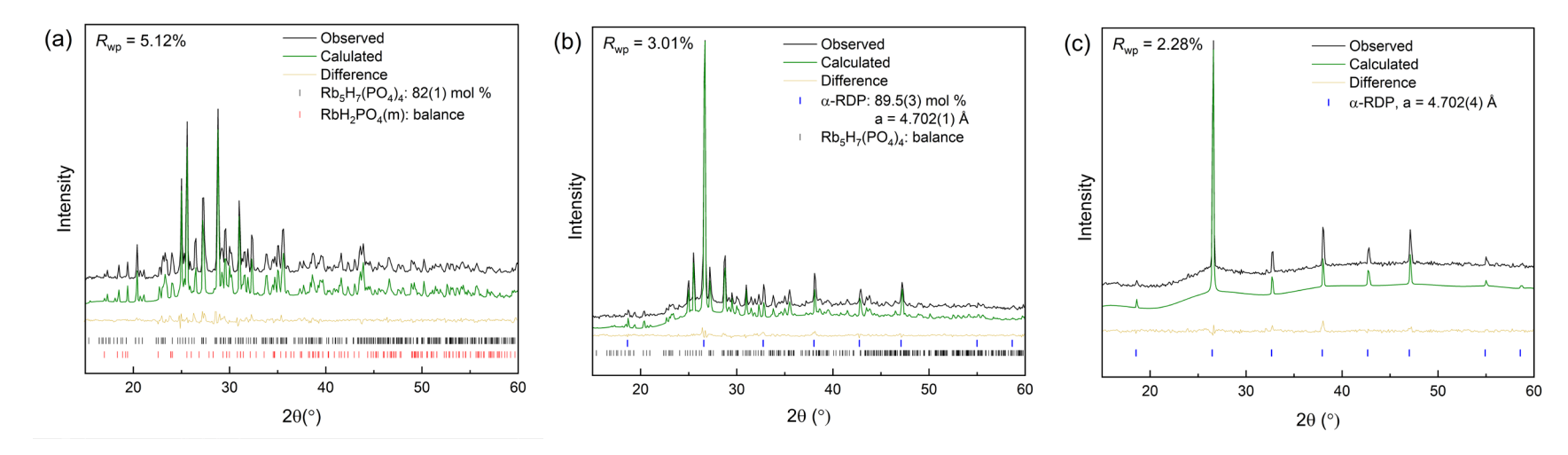


Figure 3.

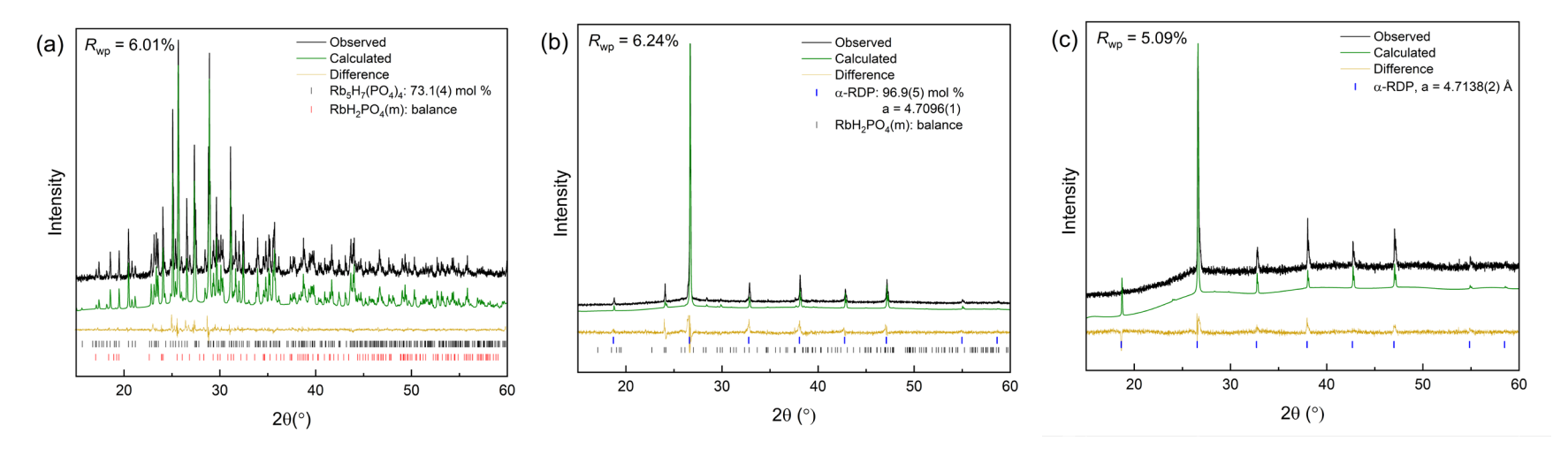


Figure 4

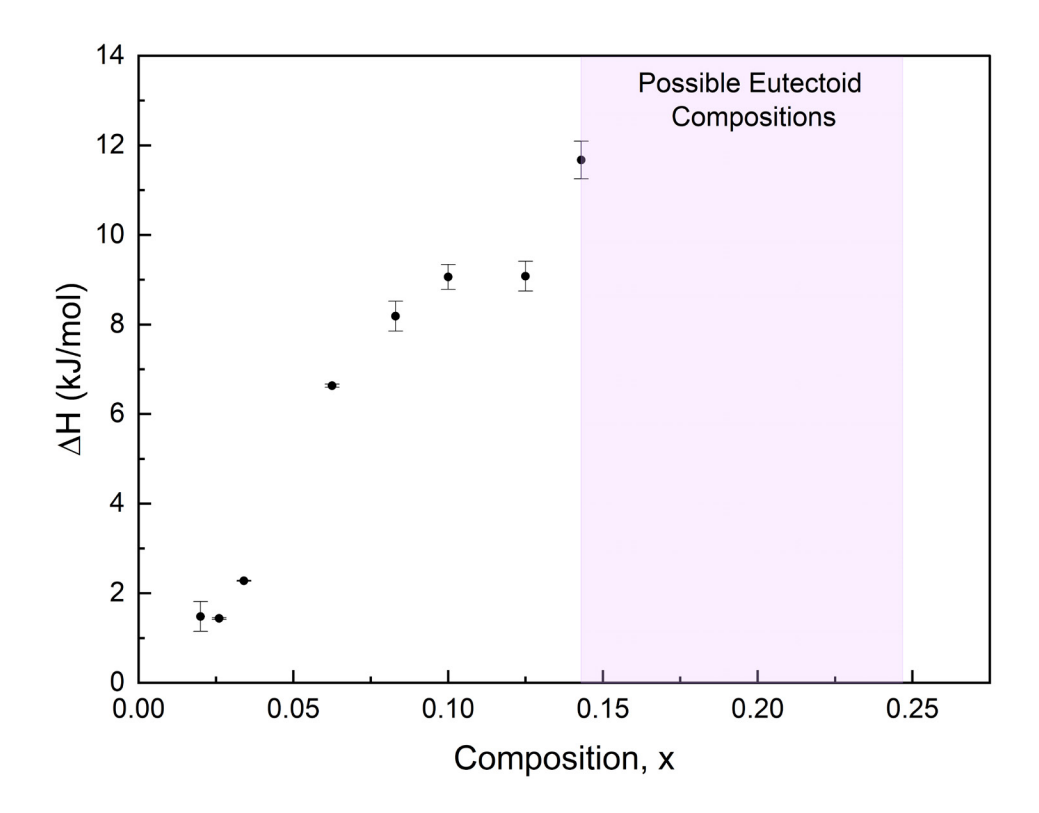


Figure 5.

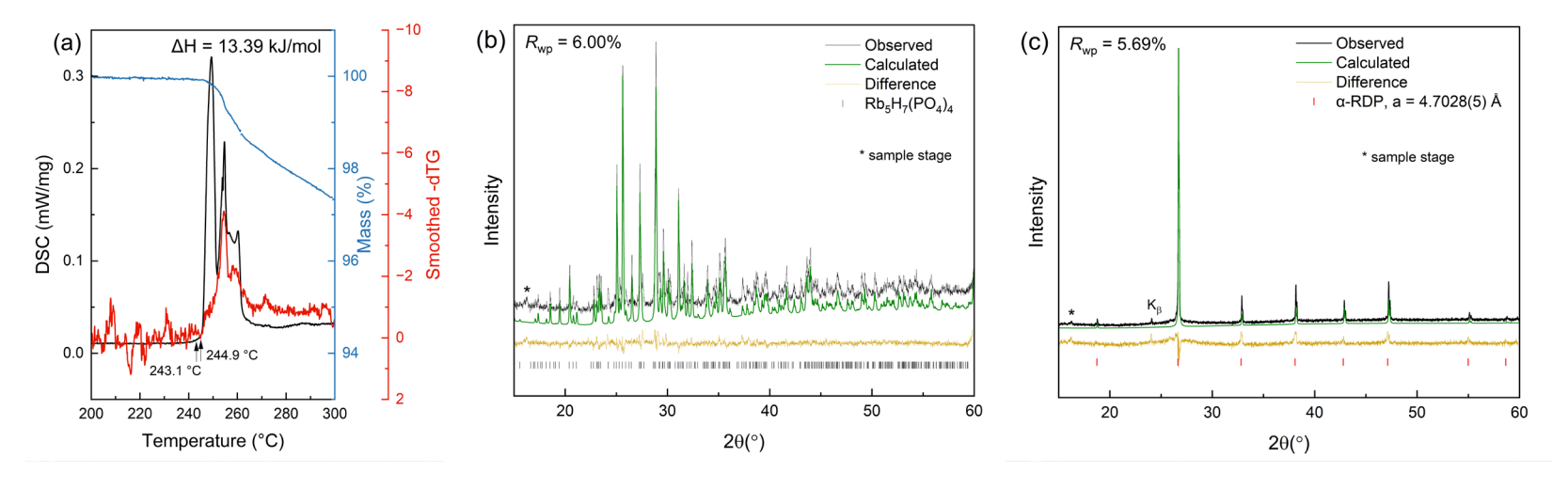


Figure 6

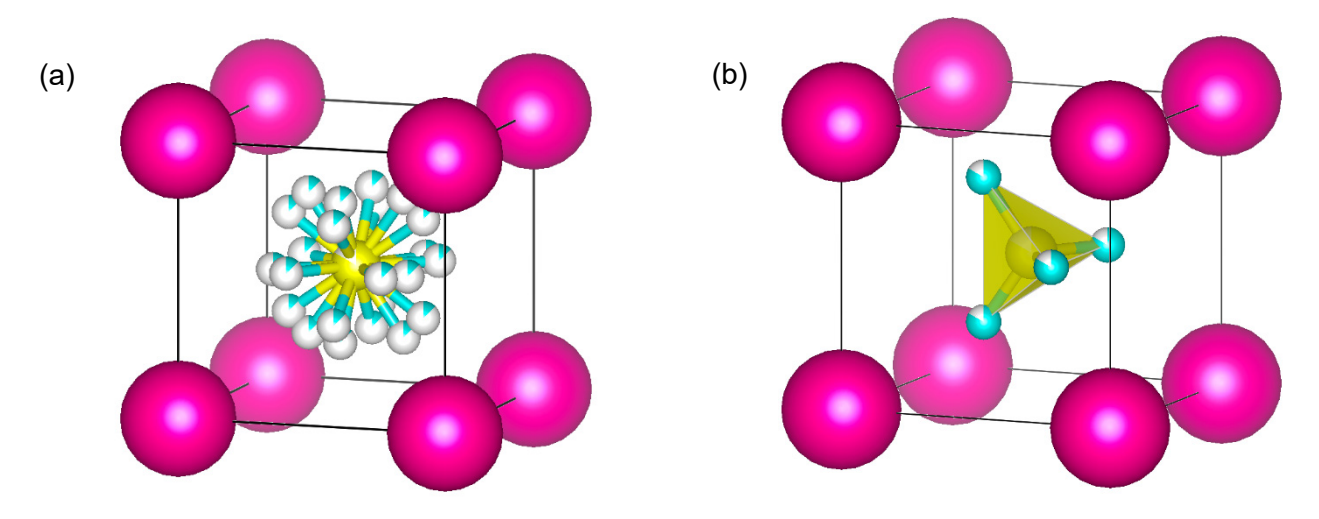


Figure 7

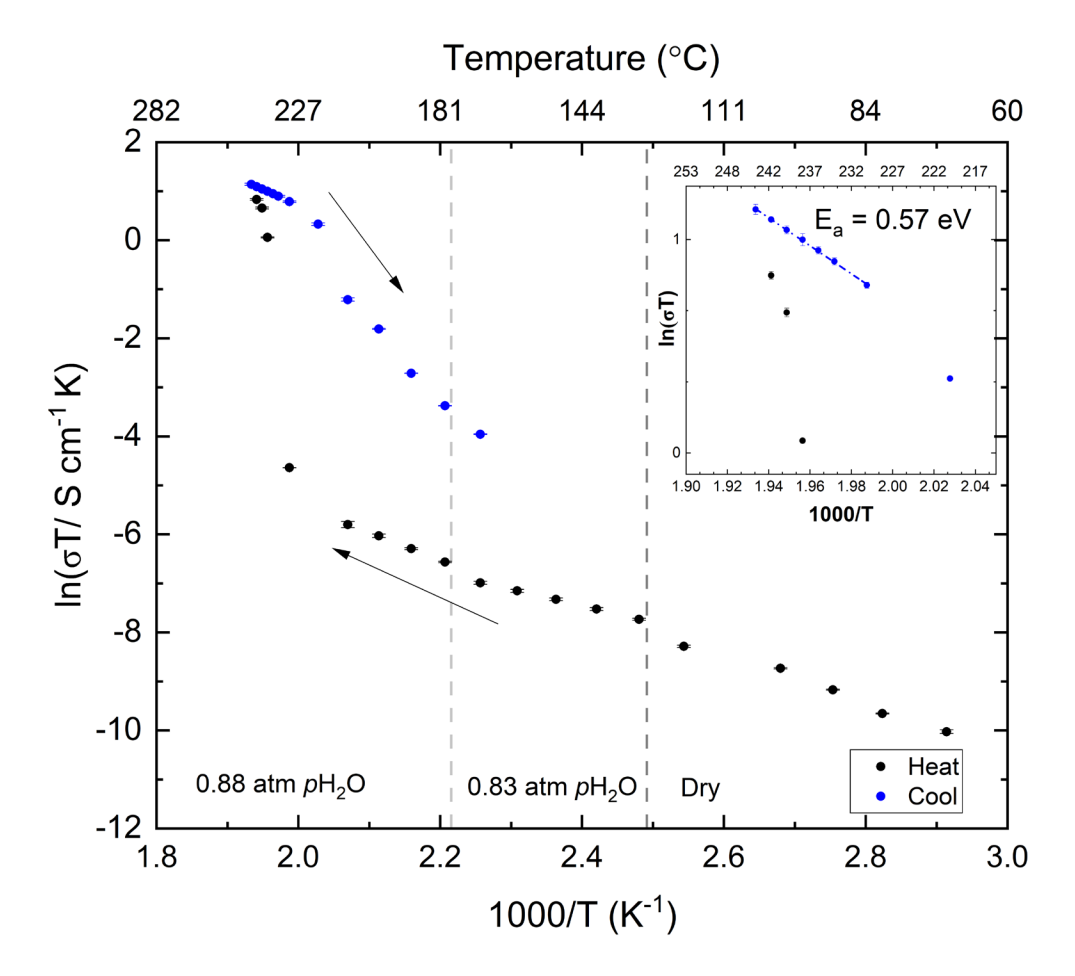
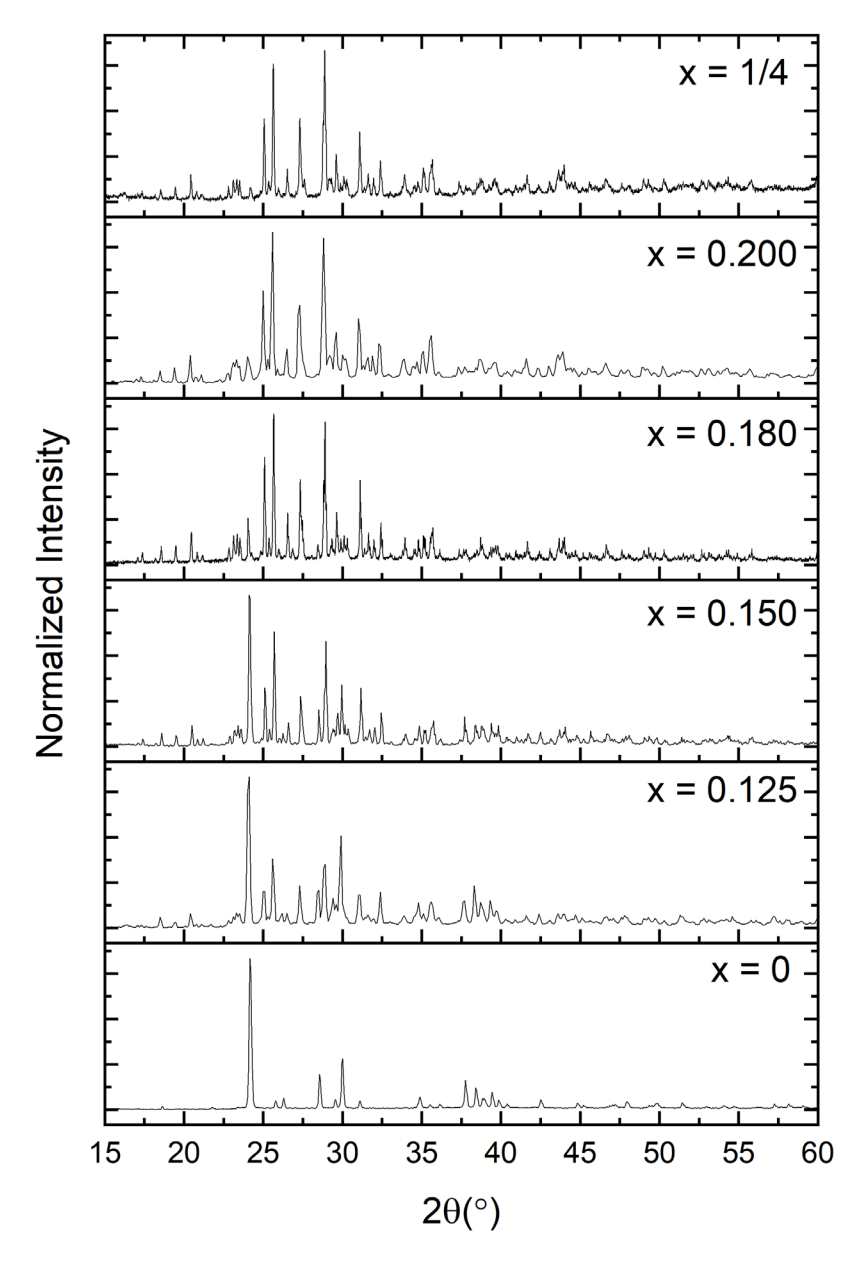


Figure 8.

# Supplementary Information

Superprotonic Conductivity in  $RbH_{2-3y}(PO_4)_{1-y}$ : a Phosphate Deficient Analog to Cubic  $CsH_2PO_4$  in the  $(1-x)RbH_2PO_4 - xRb_2HPO_4$  System

Grace Xiong, Louis S. Wang, and Sossina M. Haile



**Figure S1.** Diffraction patterns of materials in the (1-x) RbH<sub>2</sub>PO<sub>4</sub> – x Rb<sub>2</sub>HPO<sub>4</sub> system (x as indicated) at temperatures just below the eutectoid reaction temperature and pH<sub>2</sub>O = 0.83 atm. Measurement temperature is 235 °C, except for the  $x = \frac{1}{4}$  end-member (Rb<sub>5</sub>H<sub>7</sub>(PO<sub>4</sub>)<sub>4</sub>), which was measured at 237 °C. All patterns can be described as simple mixtures of RbH<sub>2</sub>PO<sub>4</sub> (monoclinic)<sup>1</sup> and Rb<sub>5</sub>H<sub>7</sub>(PO<sub>4</sub>)<sub>4</sub><sup>2</sup>. Uncertainty in the composition is 0.003.

**Table S1.** Refined lattice parameters and phase fractions from high temperature x-ray diffraction measurements at T = 235 °C at specified values of x in (1-x) RbH<sub>2</sub>PO<sub>4</sub> – x Rb<sub>2</sub>HPO<sub>4</sub> materials. For  $x = \frac{1}{4}$ , the pattern was measured at 237 °C. Atomic coordinates and isotropic atomic displacement parameters of Rb<sub>5</sub>H<sub>7</sub>(PO<sub>4</sub>)<sub>4</sub> and RbH<sub>2</sub>PO<sub>4</sub> (m) were fixed at the values reported in studies by Averbuch-Pouchot et al.<sup>2,1</sup> The cell parameters are found to be independent of the global composition, indicating the mutual insolubility of the two phases. The inconsistency between refined and expected phase fractions is attributed to challenges in obtaining truly random orientations of the crystallites in the composite samples, particularly because excessive grinding and pressing were avoided due to the tendency of the Rb<sub>5</sub>H<sub>7</sub>(PO<sub>4</sub>)<sub>4</sub> phase to deliquesce under such treatment.

	Rb <sub>5</sub> H <sub>7</sub> (PO <sub>4</sub> ) <sub>4</sub>							Rb	H <sub>2</sub> PO <sub>4</sub> (r	n) *		(%)	
X	a (Å)	b (Å)	c (Å)	Vol (ų)	Molar Fraction	Expected	a (Å)	b (Å)	c (Å)	β (°)	Vol (ų)	a	GooF
0					0	0	9.559(1)	6.2544(3)	7.778(1)	108.960(3)	439.82(6)	8.43	10.09
0.125	28.577(4)	10.345(1)	6.1673(7)	1823.3(5)	0.197(3)	0.20	9.552(4)	6.2515(7)	7.782(3)	108.91(1)	439.6(1)	5.48	6.68
0.150	28.575(1)	10.3314(6)	6.1598(3)	1818.5(2)	0.308(3)	0.27	9.552(2)	6.2531(4)	7.777(1)	108.951(5)	439.41(6)	10.44	10.24
0.180	28.581(9)	10.3341(3)	6.1625(1)	1820.2(1)	0.731(4)	0.39	9.551(5)	6.2577(7)	7.794(3)	108.98(1)	440.54(6)	6.01	7.33
0.200	28.593(3)	10.335(1)	6.1626(6)	1821.2(5)	0.82(1)	0.50	9.53(1)	6.216(3)	7.81(1)	108.93(4)	438.0(2)	5.15	6.57
1/4	28.585(1)	10.3352(4)	6.1622(2)		1	1						6.00	5.25

<sup>\*</sup>The refined molar fraction of RbH<sub>2</sub>PO<sub>4</sub> (m) is simply 1 – (refined molar phase fraction of Rb<sub>5</sub>H<sub>7</sub>(PO<sub>4</sub>)<sub>4</sub>).

**Table S2.** Refined lattice parameters of  $RbH_2PO_4(m)$  from high temperature x-ray powder diffraction measurements of the single-phase material. Atomic coordinates and isotropic atomic displacement were fixed at the values reported by Averbuch-Pouchot et al.<sup>1</sup>

Temperature (°C)	a (Å)	b (Å)	c (Å)	β (°)	Vol (ų)	Rwp (%)	GooF
125	9.5950(5)	6.19098(8)	7.7270(3)	109.238(1)	433.37(1)	8.49	10.08
145	9.5923(5)	6.19916(8)	7.7351(3)	109.201(1)	434.37(1)	8.44	10.05
165	9.592(3)	6.2031(4)	7.746(2)	109.218(5)	435.26(9)	13.97	16.58
175	9.587(2)	6.2133(4)	7.747(1)	109.142(5)	436.00(8)	12.24	14.54
185	9.580(2)	6.2192(4)	7.756(1)	109.108(5)	436.69(8)	12.03	14.29
195	9.581(2)	6.2249(3)	7.761(1)	109.099(4)	437.41(6)	10.31	12.27
205	9.571(2)	6.2320(3)	7.760(1)	109.048(4)	437.58(6)	9.19	10.91
215	9.572(1)	6.2394(3)	7.767(1)	108.992(3)	438.66(6)	9.25	11.05
225	9.564(1)	6.2474(3)	7.774(1)	108.989(3)	439.29(6)	8.59	10.27
235	9.559(1)	6.2544(3)	7.778(1)	108.960(3)	439.82(6)	8.43	10.09
245	9.556(1)	6.2619(2)	7.787(1)	108.934(3)	440.81(5)	7.92	9.47
250	9.553(1)	6.2647(2)	7.787(1)	108.914(3)	440.88(5)	7.09	8.44

**Table S3.** Refined lattice parameters of Rb<sub>5</sub>H<sub>7</sub>(PO<sub>4</sub>)<sub>4</sub> from high temperature x-ray powder diffraction measurements of the single-phase material. Atomic coordinates and isotropic atomic displacement parameters were fixed at the values reported by Averbuch-Pouchot et al.<sup>2</sup>

Temperature (°C)	a (Å)	b (Å)	c (Å)	Vol (ų)	Rwp (%)	GooF
65	28.4905(9)	10.2675(3)	6.0920(1)	1782.0(1)	4.97	4.34
155	28.546(1)	10.3025(4)	6.1266(2)	1801.8(2)	5.18	4.53
185	28.556(1)	10.3137(4)	6.1393(2)	1808.2(2)	5.45	4.77
237	28.585(1)	10.3352(4)	6.1622(2)	1820.5(2)	6.00	5.25
242	28.588(1)	10.3378(5)	6.1647(2)	1821.9(2)	5.80	5.07
245	28.589(1)	10.3391(6)	6.1663(3)	1822.7(2)	6.58	5.70

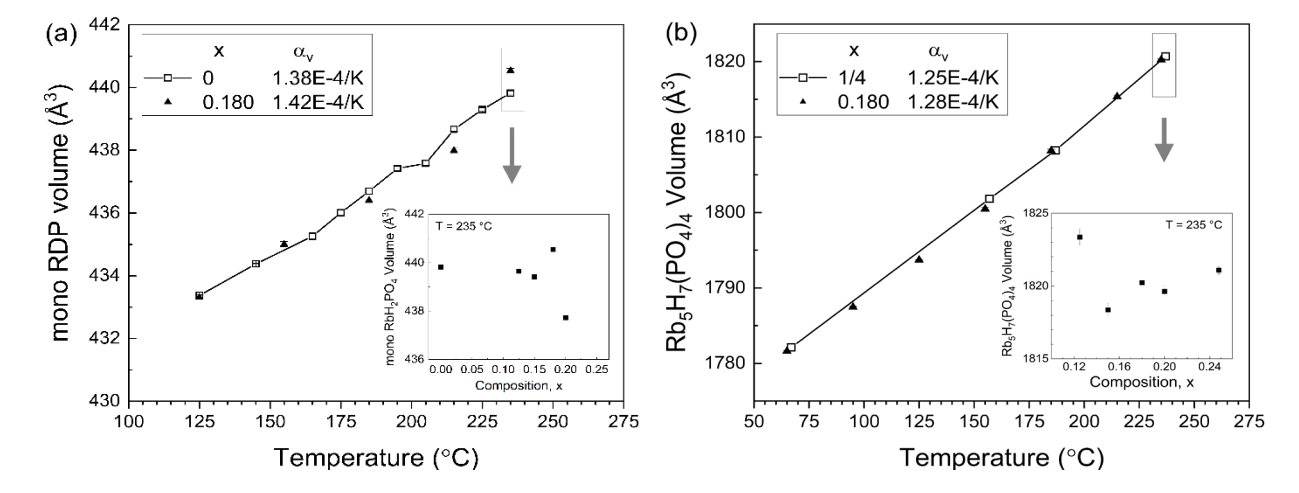


**Figure S2.** Comparison of volumes in single-phase and mixed phase systems of (a) monoclinic RbH<sub>2</sub>PO<sub>4</sub>, and (b) orthorhombic Rb<sub>5</sub>H<sub>7</sub>(PO<sub>4</sub>)<sub>4</sub> (as measured below the eutectoid temperature). At 125 °C and lower, monoclinic RbH<sub>2</sub>PO<sub>4</sub> often occurred along with its tetragonal form; only the monoclinic results are reported here. The volumes of the phases are approximately independent of the global composition, x, in (1-x) RbH<sub>2</sub>PO<sub>4</sub> – x Rb<sub>2</sub>HPO<sub>4</sub> (see insets), indicating that RbH<sub>2</sub>PO<sub>4</sub> and Rb<sub>5</sub>H<sub>7</sub>(PO<sub>4</sub>)<sub>4</sub> remain stoichiometric, that is, they are mutually insoluble, up to the eutectoid temperature (242.0±0.5 °C).

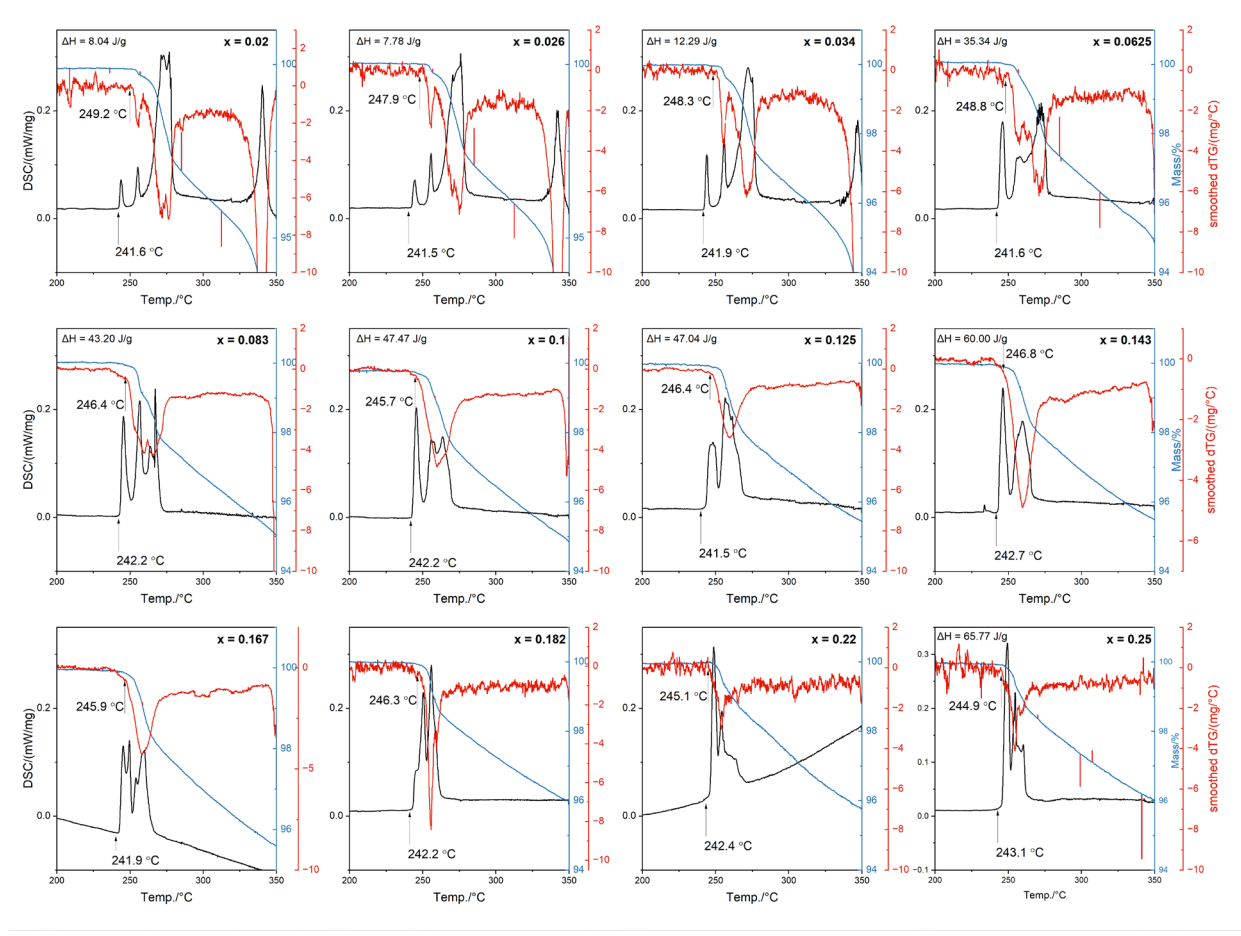


**Figure S3.** Simultaneous DSC/TGA measurement of materials in the (1-x) RbH<sub>2</sub>PO<sub>4</sub> – x Rb<sub>2</sub>HPO<sub>4</sub> system at the compositions indicated and pH<sub>2</sub>O = 0.7 atm; the composition x = 0.22 was measured with pH<sub>2</sub>O = 0.6 atm. The average eutectoid phase transition temperature is 242.0 °C with a standard deviation of 0.5 °C. Dehydration at a slightly higher temperature occurs as a distinct thermal event for low x values and overlaps with the eutectoid transition at x > 0.14. At x =  $\frac{1}{4}$ , the end-member Rb<sub>5</sub>H<sub>7</sub>(PO<sub>4</sub>)<sub>4</sub> undergoes a stoichiometric phase transition at a temperature just above that at which the eutectoid transformation occurs.

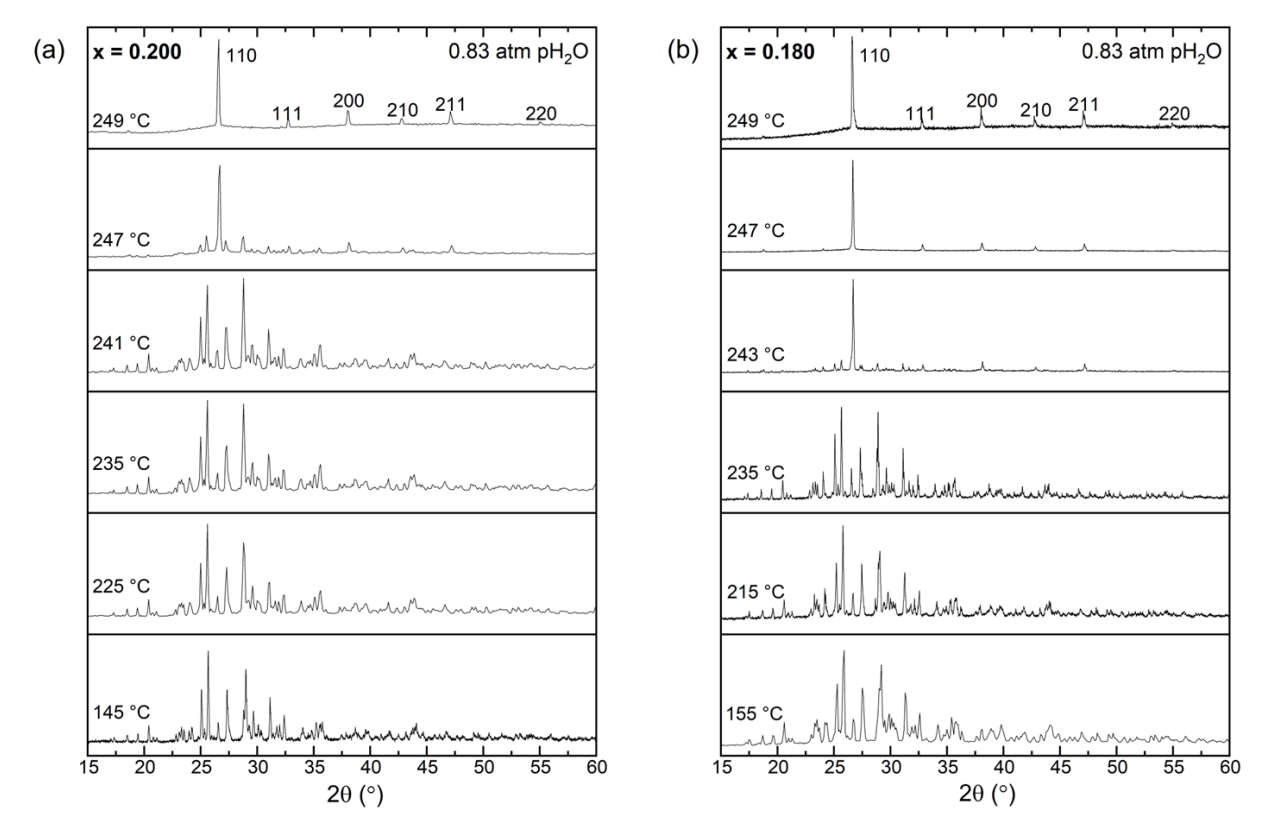


**Figure S4.** Diffraction patterns for (a) x = 0.200 and (b) x = 0.180 materials in the (1-x) RbH<sub>2</sub>PO<sub>4</sub> – x Rb<sub>2</sub>HPO<sub>4</sub> system. At high temperature, the materials transform to a phase with simple cubic structure.

**Table S4.** Refined lattice parameters and phase fractions from high temperature x-ray diffraction analysis of composition x = 0.200 in the (1-x) RbH<sub>2</sub>PO<sub>4</sub> – x Rb<sub>2</sub>HPO<sub>4</sub> system (Figure S4a). Atomic coordinates and isotropic atomic displacement parameters of Rb<sub>5</sub>H<sub>7</sub>(PO<sub>4</sub>)<sub>4</sub> and RbH<sub>2</sub>PO<sub>4</sub>(m) were fixed at the values reported by Averbuch-Pouchot et al.<sup>2,1</sup> The insensitivity of the refined molar fraction to temperature below the eutectoid transition, despite being larger than the expected value of 0.5, is consistent with mutual insolubility between Rb<sub>5</sub>H<sub>7</sub>(PO<sub>4</sub>)<sub>4</sub> and RbH<sub>2</sub>PO<sub>4</sub> (m).

.e ( <sub>o</sub> C)		Rb <sub>5</sub>	H <sub>7</sub> (PO <sub>4</sub> ) <sub>4</sub>				Rb		(0)			
Temperature (°C)	a (Å)	b (Å)	c (Å)	Vol (ų)	Molar Fraction	a (Å)	b (Å)	c (Å)	β (°)	Vol (ų)	Rwp (%)	GooF
145	28.536(2)	10.297(8)	6.128(5)	1801.0(4)	0.83(1)	9.58(3)	6.235(4)	7.72(2)	109.02(7)	436.5(3)	5.19	6.57
225	28.579(2)	10.3272(9)	6.1559(5)	1816.9(4)	0.80(1)	9.57(2)	6.238(2)	7.75(1)	109.03(4)	437.8(2)	5.01	6.37
235	28.593(3)	10.335(1)	6.1626(6)	1821.2(5)	0.82(1)	9.53(1)	6.216(3)	7.81(1)	108.93(4)	438.0(2)	5.15	6.57
241	28.590(2)	10.3340(9)	6.1630(5)	1820.8(4)	0.83(1)	9.56(2)	6.239(3)	7.75(1)	108.98(5)	438.04(3)	5.12	6.52

<sup>\*</sup> The refined mole fraction of RbH<sub>2</sub>PO<sub>4</sub> is simply 1 – (refined molar phase fraction of Rb<sub>5</sub>H<sub>7</sub>(PO<sub>4</sub>)<sub>4</sub>).

(C)	<b>Rb</b> ₅H <sub>7</sub> (PO <sub>4</sub> ) <sub>4</sub>						α-RDP (c)*									
Temperature (	a (Å)	b (Å)	c (Å)	Vol (ų)	Molar Fraction	a (Å)	Vol (ų)	Оу	Oz	P-O dist. (Å)	Uiso Rb $({ m \AA}^2)$	Uiso P ( $^4$ 2)	Uiso O ( $^2$ )	Crystallite Size (μm)	Rwp (%)	GooF
247	28.610(3)	10.353(1)	6.1742(6)	1828.9(3)	0.105(3)	4.702(1)	104.02(4)	0.204(2)	0.369(5)	1.51(5)	0.068(2)	0.054(4)	0.058(4)	0.151(8)	3.01	3.68
249					0	4.702(4)	103.95(3)	0.188(2)	0.402(6)	1.53(5)	0.068(2)	0.054(4)	0.058(4)	0.3(2)	2.28	2.98

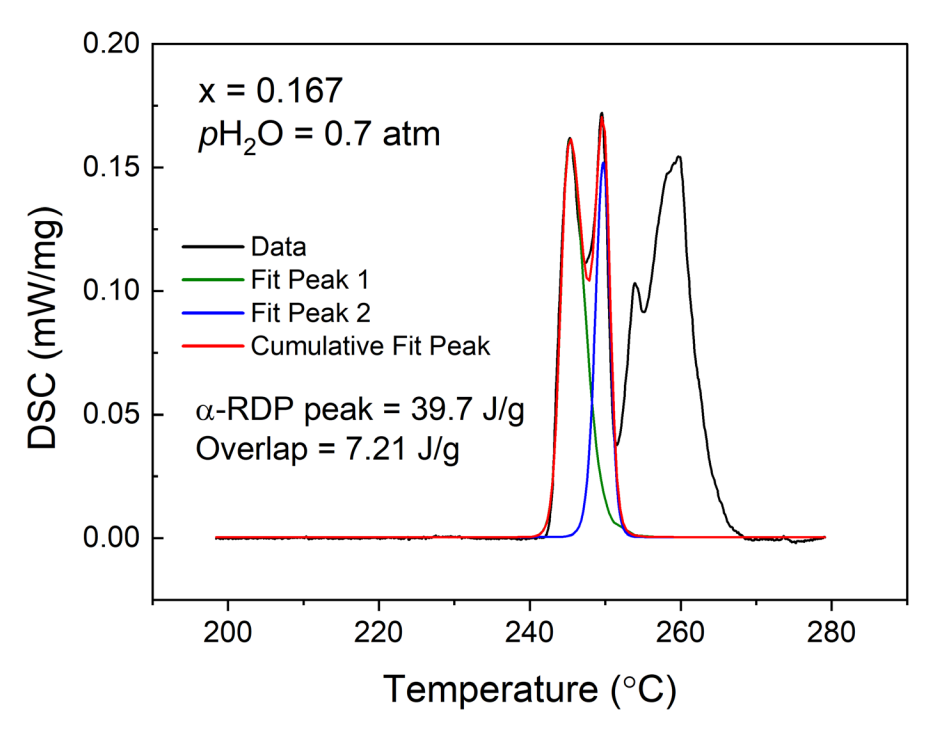
<sup>\*</sup> The refined molar fraction of  $RbH_2PO_4$  is simply  $1 - (refined molar phase fraction of <math>Rb_5H_7(PO_4)_4)$ .

**Table S5.** Refined lattice parameters and phase fractions from high temperature x-ray diffraction analysis of composition x = 0.180 in the (1-x) RbH<sub>2</sub>PO<sub>4</sub> – x Rb<sub>2</sub>HPO<sub>4</sub> system (Figure S4b).

(C)		Rb	<sub>5</sub> H <sub>7</sub> (PO <sub>4</sub>	1)4				RbH <sub>2</sub> F	O <sub>4</sub> (m)					α-R	DP (c)	*			
Temperature (°C)	a (Å)	b (Å)	c (Å)	Vol (ų)	Molar Fraction	a (Å)	b (Å)	c (Å)	β (°)	Vol (ų)	Molar Fraction	a (Å)	Vol (ų)	Оу	Oz	P-O dist. (Å)	Molar Fraction Crystallite Size (µm)	Rwp (%)	GooF
155	28.534(1)	10.2996(4)	6.1263(2)	1800.4(2)	0.687(5)	9.588(6)	6.1955(9)	7.750(3)	109.13(1)	435.00(8)	0.312(5)							7.84	9.46
185	28.556(1)	10.3133(4)	6.1396(2)	1808.1(2)	0.680(5)	9.5803(6)	6.2150(9)	7.752(3)	109.00(1)	436.41(8)	0.319(5)							7.77	9.40
215	28.571(1)	10.3252(4)	6.1535(2)	1815.3(2)	0.675(5)	9.563(6)	6.2363(8)	7.762(3)	108.90(1)	437.99(8)	0.324(5)							7.57	9.15
235	28.581(9)	10.3341(3)	6.1625(1)	1820.2(1)	0.731(4)	9.551(5)	6.2577(7)	7.794(3)	108.98(1)	440.54(6)	0.268(4)							6.01	7.33
243	28.584(2)	10.333(7)	6.1671(3)	1821.6(2)	0.072(2)	9.54(1)	6.263(2)	7.790(7)	108.99(2)	440.3(1)	0.0450(1)	4.7085(2)	104.38(1)	0.208(1)	0.376(3)	1.49(3)	0.882(2) 0.279(7)	6.59	8.02
245						9.51(1)	6.260(2)	7.78(1)	108.81(3)	439.2(1)	0.0301(1)	4.7096(1)	104.46(1)	0.203(1)	0.375(2)	1.51(2)	0.969(5) 0.292(6)	6.24	7.56
247												4.7130(1)	104.68(1)	0.211(1)	0.377(1)	1.46(1)	1 0.322(5)	4.77	5.68
249												4.7183(3)	105.07(1)	0.184(1)	0.392(3)	1.57(2)	1 0.222(6)	5.09	5.22

<sup>\*</sup>The lattice parameters, phase fractions, and  $\alpha$ -RDP crystallite size were allowed to vary freely. The displacement parameters obtained from the refinement of  $\alpha$ -RDP at x = 0.18 and 245 °C (with values of 0.068(2) Å<sup>2</sup>, 0.054(4) Å<sup>2</sup>, and 0.058(4) Å<sup>2</sup> for Rb, P, and O, respectively, see main text) were employed as fixed inputs. The oxygen position was refined with a restraint targeting a P-O bond length of 1.53 Å.

.



Asymmetric double sigmoidal curve: 
$$y = y_0 + A \frac{1}{1 + e^{\frac{x - x_c + (w_1/2)}{w_2}}} (1 - \frac{1}{1 + e^{\frac{x - x_c + (w_1/2)}{w_2}}})$$

Feature	$Y_0$	$X_{c}$	A	$\mathbf{W}_1$	$W_2$	$W_3$
Peak 1	5e-4	245.54	0.22	2.8	0.53	1.16
Peak 2	5e-4	249.7	0.22	1.65	0.6	0.45

**Figure S5.** Illustration of the high degree of overlap between the thermal event associated with the eutectoid transition and that associated with dehydration in (1-x) RbH<sub>2</sub>PO<sub>4</sub> – x Rb<sub>2</sub>HPO<sub>4</sub> compositions with large x. Attempts to distinguish contributions from the individual processes via peak fitting (as shown above) to the overlapped response yielded unsatisfactory results.

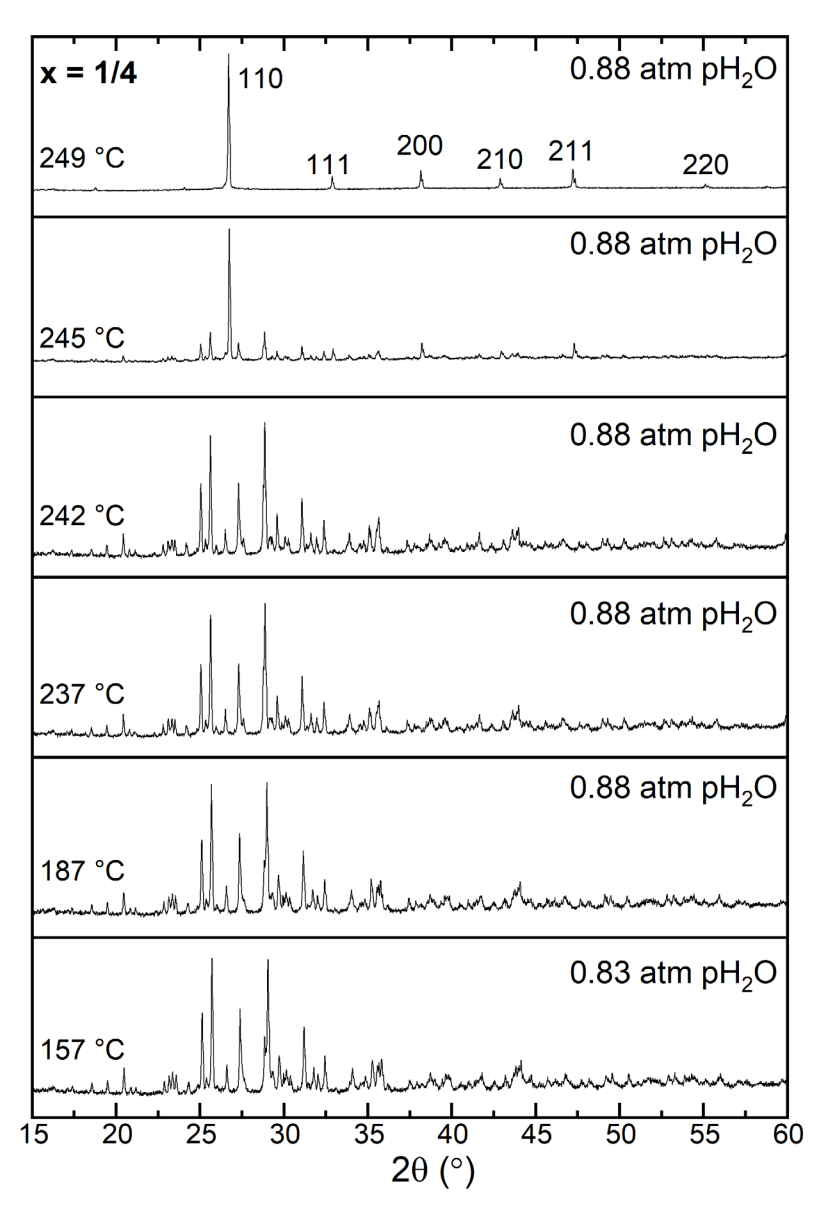


**Figure S6.** Diffraction patterns of Rb<sub>5</sub>H<sub>7</sub>(PO<sub>4</sub>)<sub>4</sub> ( $x = \frac{1}{4}$  in the (1-x)RbH<sub>2</sub>PO<sub>4</sub> – xRb<sub>2</sub>HPO<sub>4</sub> system) at the temperatures and steam partial pressures indicated. At high temperature, Rb<sub>5</sub>H<sub>7</sub>(PO<sub>4</sub>)<sub>4</sub> transforms to a phase with a simple cubic lattice. Refinement results reported in Tables S3 and S6.

**Table S6.** Refined crystallographic properties of the  $\alpha$ -RDP phase from high temperature x-ray diffraction patterns of Rb<sub>5</sub>H<sub>7</sub>(PO<sub>4</sub>)<sub>4</sub> (Figure S6).

Temperature	size								
(°C)	(μm)	a (Å)	Vol (ų)	Оу	Oz	P-O distance	Molar Fraction	Rwp%	GooF
245	0.98(6)	4.6945(1)	103.46(1)	0.195(1)	0.373(2)	1.54(2)	0.9801(2)	5.37	4.66
249	0.27(2)	4.7026(1)	104.00(1)	0.187(1)	0.371(1)	1.58(2)	1	5.69	4.89

At 249 °C the material is fully transformed to α-RDP. At 245 °C, a small amount of residual Rb<sub>5</sub>H<sub>7</sub>(PO<sub>4</sub>)<sub>4</sub> remains, attributed to thermal gradients in the high temperature stage.

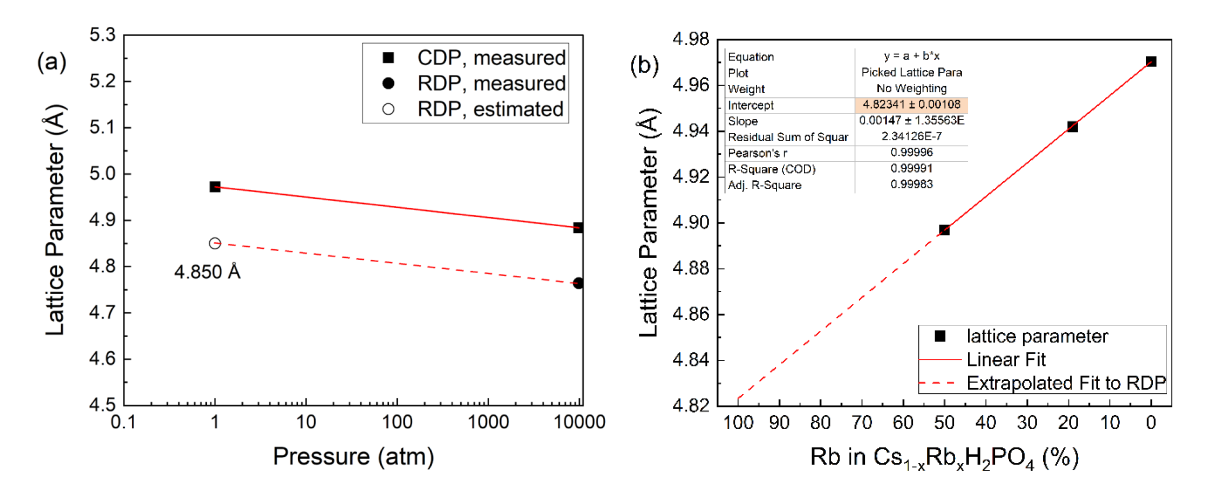


**Figure S7.** Estimation of the (hypothetical) lattice parameter of the cubic phase of RbH<sub>2</sub>PO<sub>4</sub> at 249 °C and 1 atm total pressure: (a) extrapolation from high pressure, assuming bulk modulus of CsH<sub>2</sub>PO<sub>4</sub><sup>3</sup> and (b) extrapolation from Cs<sub>1-x</sub>Rb<sub>x</sub>H<sub>2</sub>PO<sub>4</sub><sup>4</sup>.

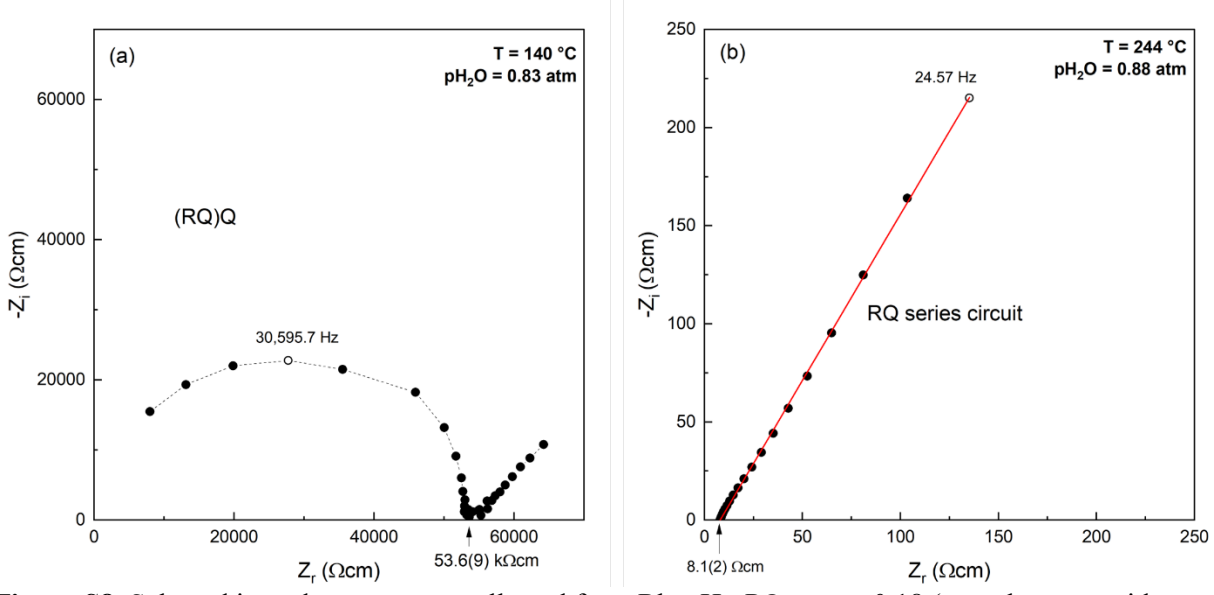


**Figure S8.** Selected impedance spectra collected from  $Rb_{1+x}H_{2-x}PO_4$  at x = 0.18 (near the eutectoid composition) at the conditions indicated. In the (a) low conductivity regime the spectra are modeled using an (RQ)Q circuit, whereas in the (b) superprotonic phase, the impedance behavior is modeled using a resistor and a Warburg impedance element in series.

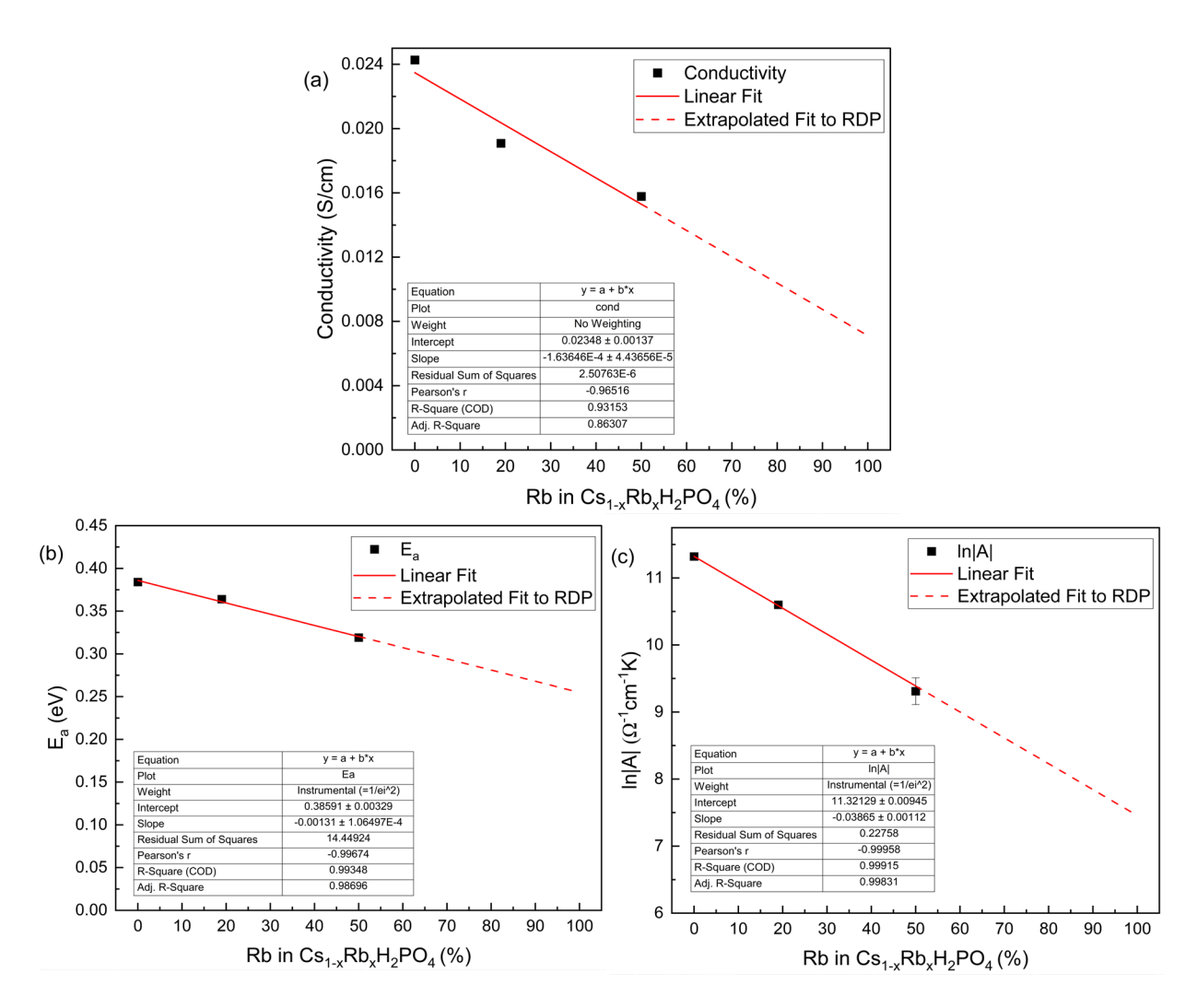


Figure S9. Estimation of (hypothetical) proton transport properties of the cubic  $RbH_2PO_4$ . The (a) conductivity at 255 °C, (b) activation energy, and (c) preexponential factor were extrapolated from reported properties of  $Cs_{1-x}Rb_xH_2PO_4^4$ . The extrapolations suggests that if stoichiometric  $RbH_2PO_4$  occurred under ambient pressures, it would display an activation energy even smaller than that of stoichiometric  $CsH_2PO_4$ , but its conductivity would be moderate due to a small value of the preexponential term. Studies of  $\alpha$ -RDP compositions with more moderate nonstoichiometry than the eutectic composition would likely shed light on the trends in Ea and ln(A) on the overall conductivity.

#### References

- 1. M. T. Averbuch-Pouchot and A. Durif, *Acta Crystallographica*, 1985, C41, 665-667.
- 2. M. T. Averbuch-Pouchot and A. Durif, *Acta Crystallographica* 1985, C41, 1555–1556.
- 3. C. E. Botez, R. J. Tackett, J. D. Hermosillo, J. Z. Zhang, Y. S. Zhao and L. P. Wang, *Solid State Ionics*, 2012, **213**, 58-62.
- 4. A. Ikeda, D. A. Kitchaev and S. M. Haile, *Journal of Materials Chemistry A*, 2014, **2**, 204-214.